Warm cloud chemistry and physics

Physics and Chemistry of the Atmosphere (ENV-320)

Cloud condensation nuclei (CCN)

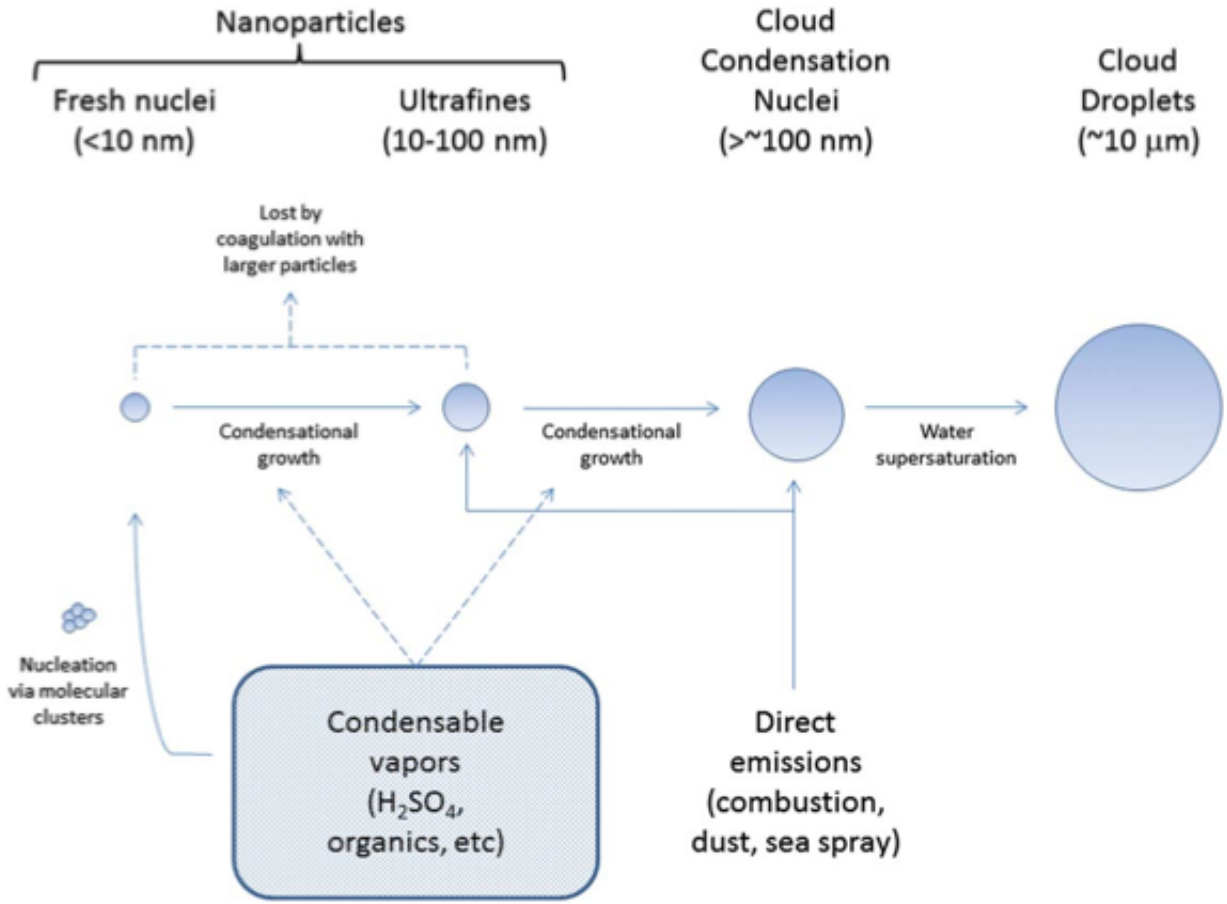

Figure 2. A schematic of processes that form cloud condensation nuclei (CCN).

Particles may either be directly emitted (primary) or nucleated in the atmosphere itself (secondary). Nucleated particles (1–2 nm dia.) must grow substantially via condensation of sulfuric acid and organics to approximately ~100 nm dia. before they can nucleate cloud droplets. Along the way, many of the nucleated particles are lost by coagulating with pre-existing, larger particles.

Adams et al., 2013

Fig. 6.9 Ship tracks (white lines) in marine stratus clouds over the Atlantic Ocean as viewed from the NASA Aqua satellite on January 27, 2003. Brittany and the southwest coast of England can be seen on the upper right side of the image.

Cloud droplet formation

- For cloud droplets to form from nucleation of pure water vapor, a few hundred percent RH is required.
- Particles with solutes which dissolve in water are most effective in lowering the required supersaturation $\Rightarrow$ most effective as cloud condensation nuclei (solution-vapor equilibrium described by Köhler curve).
- Updrafts are caused by ground heating and topography.
  - adiabatic expansion of moist air parcels cools the air below its dew point
  - supersaturations (RH$>$100%): $\sim$0.1–1%; typically 0.1–0.3% in excess of 100% RH in the marine boundary layer
- As water vapor condenses, latent heat (of vaporization) is released, contributing to the continued buoyancy of the air parcel.

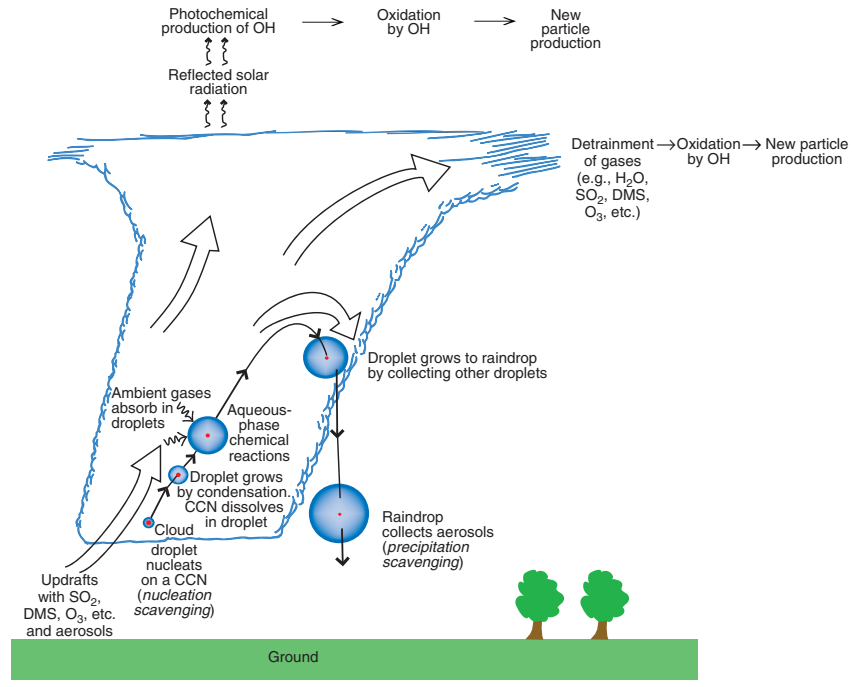

Thermodynamics of cloud droplet formation

Equilibrium vapor pressure over a curved surface (Kelvin equation). The derivation is general, but the application area will be for water vapor.

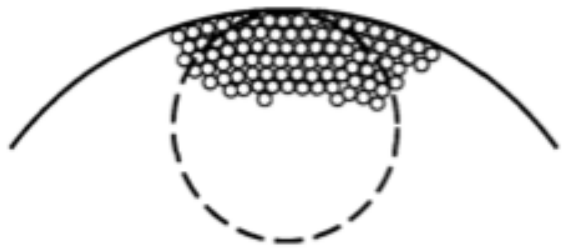

FIGURE 10.11 Effect of radius of curvature of a drop on its vapor pressure.

- Physical interpretation of Kelvin effect: less neighboring molecules at the surface (less resistance against escape from attractive forces) leads to higher rate of evaporation.
- Vapor pressure over a curved surface is therefore always higher than over a flat one.

We will also derive an expression for the saturation vapor pressure over a droplet solution (Köhler equation).

Free energy of formation of droplet from pure vapor (for this application, G is equivalent to the energy defined by E in Wallace and Hobbs, 2006):

$$\Delta G = G_{\text{final}} - G_{\text{initial}} = G_{\text{droplet}} - G_{\text{pure vapor}}$$

Definitions:

- Total number of molecules is N_T, initially in the vapor phase.
- After partitioning, N_l molecules are in the droplet phase and $N_v = N_T - N_l$ molecules remain in the vapor phase.
- g is the molecular Gibbs free energy ($g = G/N$).
- $4\pi r^2\sigma$ is the free energy associated with the radius of curvature r and surface tension σ. Note that surface tension is related to surface energy (energy per unit surface area, J/cm^2).

We then get

$$\Delta G = N_v g_v + N_l g_l + 4\pi r^2\sigma - N_T g_v = 4\pi r^2\sigma + N(g_l - g_v)$$

The change in (molecular) Gibbs free energy as a function of pressure at constant temperature is given by the thermodynamic relation,

$$dg = vdp$$

where v is the molecular volume ($v = V/N$). Integrating over initial (vapor-phase) to final (droplet) states,

$$g_l - g_v = \int_{p=e_s}^{e} (v_l - v_v)dp$$

where e and T are the actual vapor pressure and temperature of the system, and e_s is saturation vapor pressure over flat surface. Since $v_v \gg v_l$ and $v_v = kT/p$ (ideal gas law for molecular rather than mole basis),

$$g_l - g_v = -kT \ln \frac{e}{e_s}$$

The total number of molecules in the droplet N_l is equal to the droplet volume V_l times the number concentration of molecules per unit volume of droplet n:

$$N_l = nV_l = n\frac{4}{3}\pi r^3$$

Therefore,

$$\Delta G = 4\pi r^2\sigma - \frac{4}{3}\pi r^3 nkT \ln\frac{e}{e_s}$$

Recall the saturation ratio $S = e/e_s$.

- ΔG monotonically increases with r for subsaturated ($S < 1$) conditions.
- ΔG exhibits a maximum with respect to r for supersaturated ($S > 1$) conditions.

Under supersaturated conditions, the critical radius r^*, which corresponds to the metastable point ΔG^* (or ΔE^*), is found by solving for $d\Delta G(r^*)/dr = 0$.

$$r^* = \frac{2\sigma}{nkT \ln\frac{e}{e_s}}$$

We can examine the direction for spontaneous change from the sign of $d\Delta G(r)/dr$.

- When $r < r^*$: droplets tend to evaporate
- When $r > r^*$: droplets will grow spontaneously

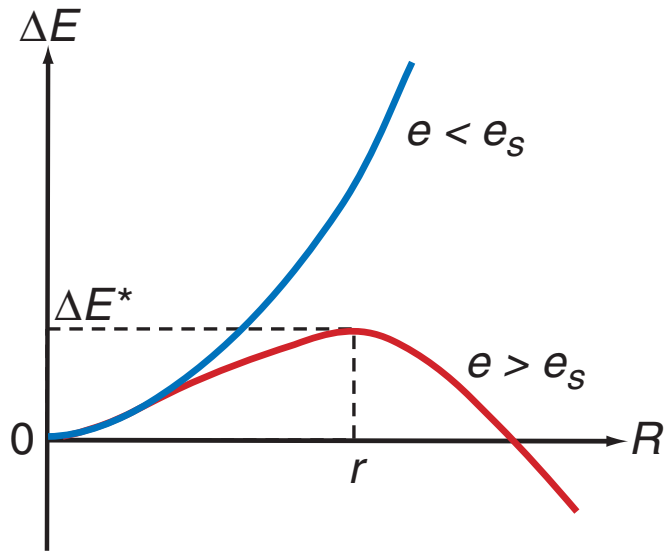

Fig.6.1 Increase ΔE in the energy of a system due to the formation of a water droplet of radius R from water vapor with pressure e; e_s is the saturation vapor pressure with respect to a plane surface of water at the temperature of the system.

The Kelvin equation is derived from the expression for the critical radius:

$$e(r^*) = e_s \exp\left(\frac{2\sigma}{nkTr^*}\right)$$

Henceforth dropping the * (we can choose to represent this variable with any symbol, for which we again choose r): $e(r) = e_s \exp\left(\frac{2\sigma}{nkTr}\right)$. This can also be expressed as

$$e(r) = e_s \exp\left(\frac{2\sigma M_w}{RT\rho_w r}\right)$$

where we have additionally specified molecular and bulk properties of pure water

- M_w is the molecular weight of water
- ρ_w is the liquid-phase mass density (note we have switched to the use of the gas constant, R, in place of the Boltzmann constant, k).

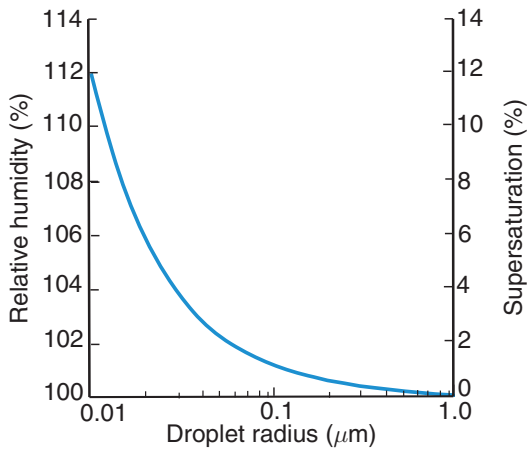

Fig. 6.2 The relative humidity and supersaturation (both with respect to a plane surface of water) at which pure water droplets are in (unstable) equilibrium at 5 °C.

The supersaturation required to generate a stable embryo (critical nucleus) homogeneously is immensely large (several hundred percent). Requires seeding (*cloud condensation nuclei*).

Vapor pressures of water:

- e_s = vapor pressure of pure water over a flat surface
- $e = e(r)$ = vapor pressure of pure water over a curved surface
- $e(r) = e'$ = vapor pressure of water containing dissolved solutes, over a curved surface

Recall Raoult's law, previously written as $p_i = x_i p_i^*$. We will use the notation $e' = p_{\text{water}}$ for the vapor pressure, $e = p^*_{\text{water}}$ for the pure component vapor pressure, and $f = x_{\text{water}}$ for the mole fraction of water.

$$\frac{e'}{e} = f$$

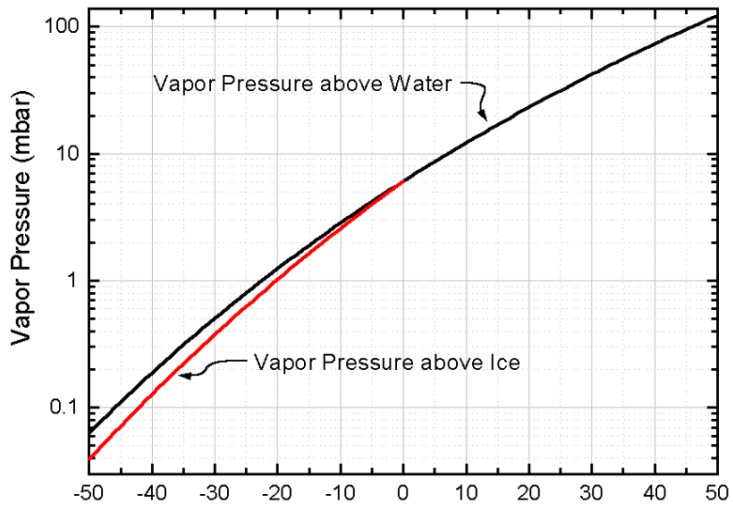

http://www.its.caltech.edu/ atomic/snowcrystals/ice/ice.htm

Let

- ρ' = density of the solution,
- r = droplet radius,
- M_w = molecular weight of water,
- m_i = mass of dissolved solute i with molecular weight M_i, and
- Φ_i = van't Hoff factor (number of dissociated ions per mole of solute). Note that this is written as i in the textbook.

The mole fraction of water containing a single dissolved solute is

$$f = \frac{\left(\frac{4}{3}\pi r^3 \rho' - m_i\right)/M_w}{\left(\frac{4}{3}\pi r^3 \rho' - m_i\right)/M_w + \Phi_i m_i / M_i}$$

$$= \left[1 + \frac{\Phi_i m_i M_w}{M_i\left(\frac{4}{3}\pi r^3 \rho' - m_i\right)}\right]^{-1}$$

We previously derived the expression for e/e_s; we replace σ and n with σ' (surface energy of solution) and n' (number concentration of water molecules):

$$\frac{e'}{e_s} = \frac{e'}{e}\frac{e}{e_s} = \left[1 + \frac{\Phi_i m_i M_w}{M_i\left(\frac{4}{3}\pi r^3 \rho' - m_i\right)}\right]^{-1} \exp\left(\frac{2\sigma'}{n' kTr}\right)$$

This equation describes the dependence of the relative humidity/saturation ratio in equilibrium with a droplet as a function of its size (*Köhler curve*). Note that the saturation ratio for water vapor in equilibrium with a solution is $S = e'/e_s$.

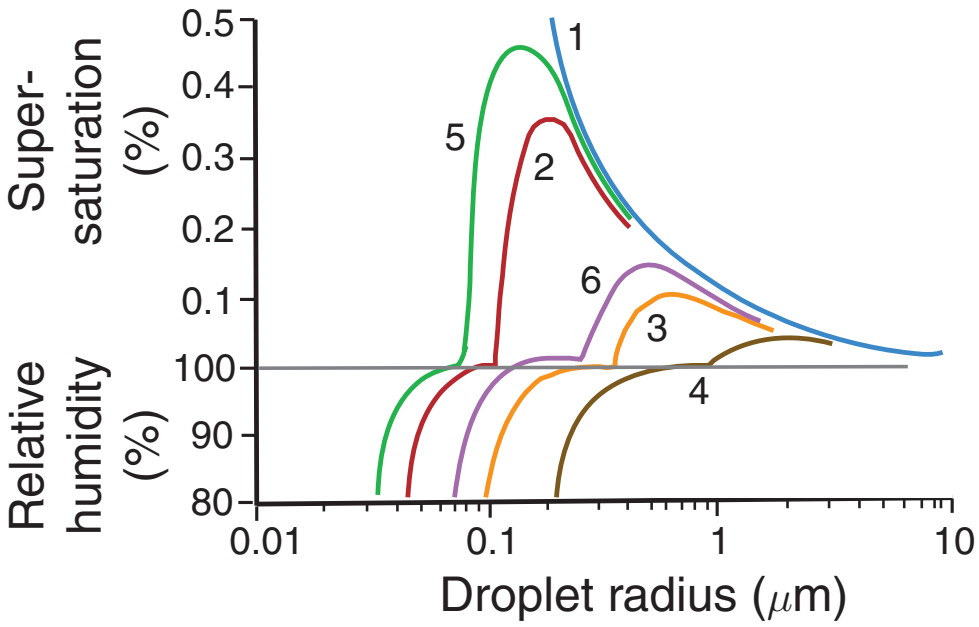

Fig. 6.3 Variations of the relative humidity and supersaturation adjacent to droplets of
(1) pure water (blue)
and adjacent to solution droplets containing the following fixed masses of salt:
(2) 10^{-19} kg of NaCl,
(3) 10^{-18} kg of NaCl,
(4) 10^{-17} kg of NaCl
(5) 10^{-19} kg of $(NH_4)_2SO_4$, and
(6) 10^{-18} kg of $(NH_4)_2SO_4$.
Note the discontinuity in the ordinate at 100% relative humidity.

Alternate form of the Köhler equation

We can present the Köhler equation in another form to make the size dependence of the curvature and solute effects more salient. We can write:

$$\frac{e}{e_s} = \frac{e'}{e_s}\frac{1}{f} = \exp\left(\frac{2\overline{v}_w\sigma'}{RTr}\right)$$

$\overline{v}_i$ is the partial molar volume $\partial V/\partial n_i$ where n_i is the number of moles of substance i. The total drop volume can be defined in terms of partial molar volumes:

$$\frac{4}{3}\pi r^3 = n_w\overline{v}_w + n_s\overline{v}_s$$

Note that $n_s = \Phi_i m_i/M_i$, or, more generally, $n_s = \sum_i \Phi_i m_i/M_i$, and $\overline{v}_s$ its corresponding partial molar volume.

$$\frac{1}{f} = 1 + \frac{n_s}{n_w} = 1 + \frac{n_s\overline{v}_w}{4/3\,\pi r^3 - n_s\overline{v}_s}$$

$$\ln\left(\frac{e'}{e_s}\right) = \frac{2\overline{v}_w\sigma'}{RTr} - \ln\left(1 + \frac{n_s\overline{v}_w}{4/3\,\pi r^3 - n_s\overline{v}_s}\right)$$

The volume occupied by the solute is small compared to the droplet volume: $n_s \overline{v}_s \ll 4/3\,\pi r^3$ and $\overline{v}_w \approx M_w/\rho_w$:

$$\ln\left(\frac{e'}{e_s}\right) = \frac{2\overline{v}_w\sigma'}{RTr} - \ln\left(1 + \frac{3n_sM_w}{4\pi\rho_w r^3}\right)$$

Mathematical property: $\ln(1+x) \to x$ as $x \to 0$ (dilute solution), so

$$\ln\left(\frac{e'}{e_s}\right) = \frac{2\overline{v}_w\sigma'}{RTr} - \frac{3n_sM_w}{4\pi\rho_w r^3}$$

If we let

$$a = \frac{2\overline{v}_w\sigma'}{RT} \text{ and } b = \frac{3n_sM_w}{4\pi\rho_w}$$

then

$$\ln\left(\frac{e'}{e_s}\right) = \frac{a}{r} - \frac{b}{r^3}$$

where

$$a/r = \text{curvature effect}$$

$$b/r^3 = \text{solute effect}$$

Illustration

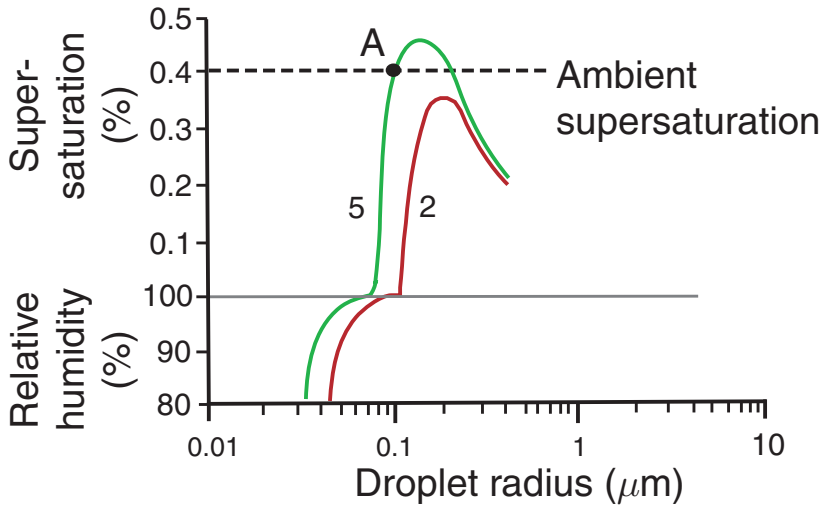

Fig. 6.4 Köhler curves 2 and 5 from Fig. 6.3. Curve 2 is for a solution droplet containing 10^{-19} kg of NaCl, and curve 5 is for a solution droplet containing 10^{-19} kg of $(NH_4)_2SO_4$. The dashed line is an assumed ambient supersaturation discussed in the text.

Haze droplet. A droplet at point A is in equilibrium with its supersaturated vapor phase (with respect to water). Haze droplets in the atmosphere can considerably reduce visibility by scattering light.

Regimes:

- peak corresponds to (r_{crit}, SS_{crit})
- $r < r_{crit}$: aerosol
- $r > r_{crit}$: cloud droplet (*activated droplet*)

Compare SS_{amb}, SS_{eq}, and SS_{crit}:

- $r < r_{crit}$ and $SS_{eq} < SS_{amb} < SS_{crit}$: condensational growth will increase droplet radius and SS_{eq}; growith is terminated when $SS_{eq} = SS_{amb}$
- $r > r_{crit}$ and $SS_{crit} < SS_{amb}$: aerosol will activate into a cloud droplet
- $r > r_{crit}$ and $SS_{eq} < SS_{amb}$: growth of droplet will increase SS_{eq} and further increase the driving force for condensational flux $SS_{amb} - SS_{eq}$, until water vapor is eventually reduced ($SS_{amb} \to SS_{eq}$)

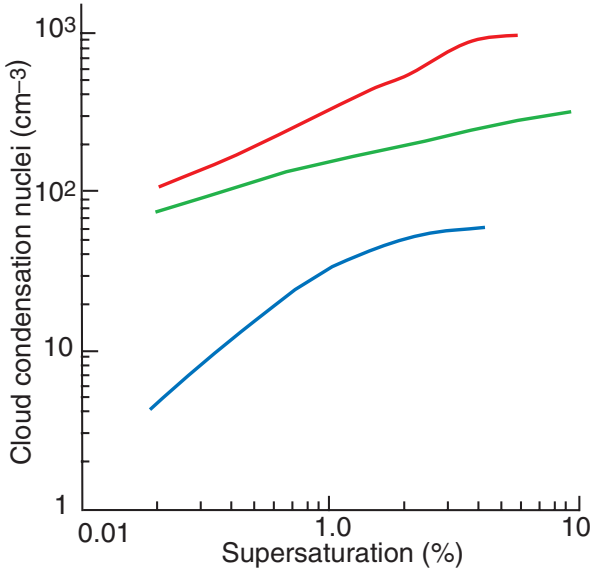

J. Geophys. Res. **107** (D19), 8022, doi:10.1029_2001JD000829, 2002.

Fig. 6.5 Cloud condensation nucleus spectra in the boundary layer from measurements near the Azores in a polluted continental air mass (brown line), in Florida in a marine air mass (green line), and in clean air in the Arctic (blue line).

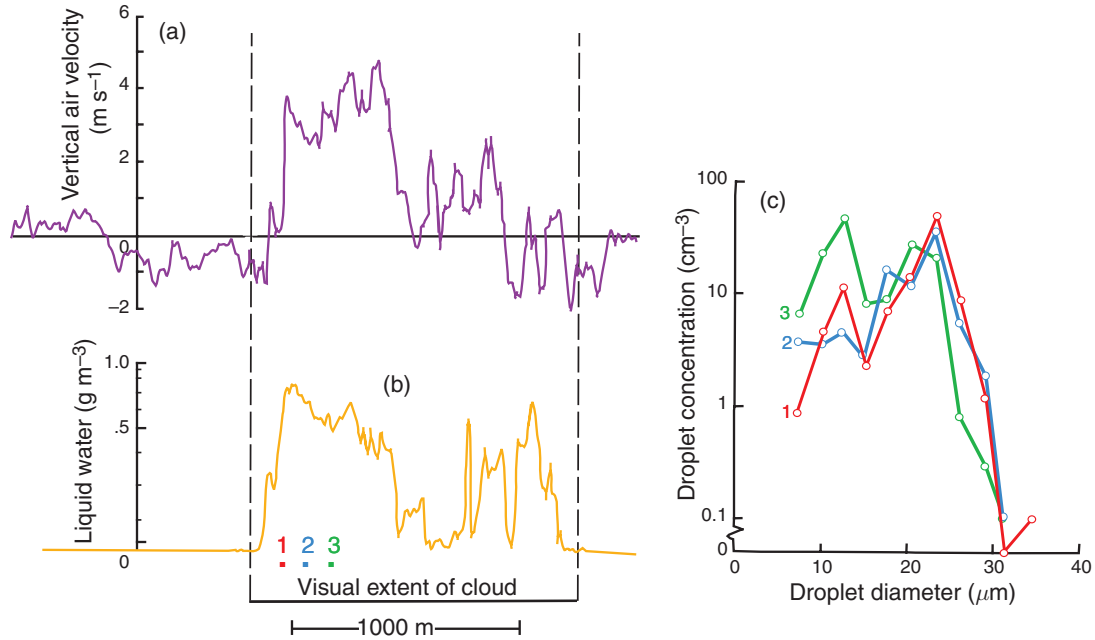

Fig. 6.6 (a) Vertical air velocity (with positive values indicating updrafts and negative values downdrafts), (b) liquid water content, and (c) droplet size spectra at points 1, 2, and 3 in (b), measured from an aircraft as it flew in a horizontal track across the width and about half-way between the cloud base and cloud top in a small, warm, nonraining cumulus cloud. The cloud was about 2 km deep.

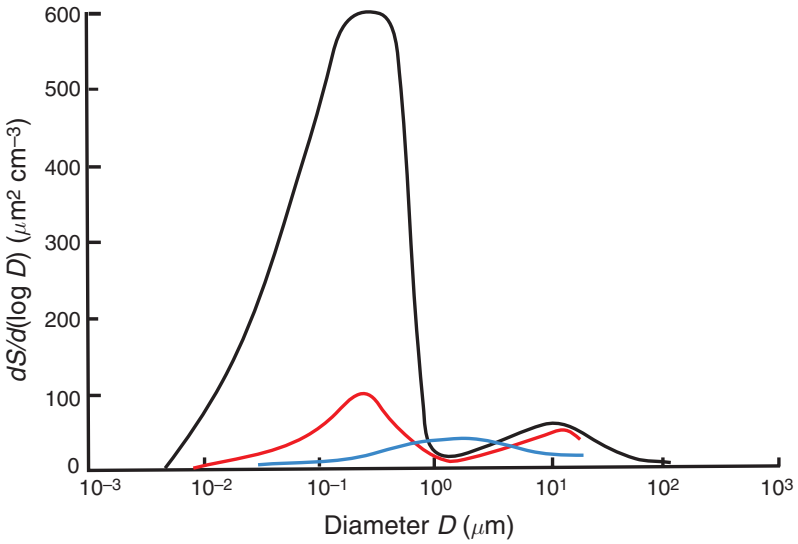

Desig-nation	Aitken nuclei	Large particles	Giant particles
Sources	Combustion; Gas-to-particle conversions; Fly ash, sea-salt, pollens; Windblown dusts; Coagulation of Aitken nuclei; Cloud droplet evaporation; Giant particles from industries		
Sinks	Coagulation; Capture by cloud particles; Precipitation scavenging; Dry fallout		
Resi-dence time	Less than an hour in polluted air or in clouds	Days to weeks	Hours to days; Minutes to hours

Fig. 5.11 Schematic curves of particle surface area distributions for urban polluted air (black line), continental air (red line), and marine air (blue line). Shown below the curves are the principal sources and sinks of atmospheric particles and estimates of their mean residence times in the troposphere.

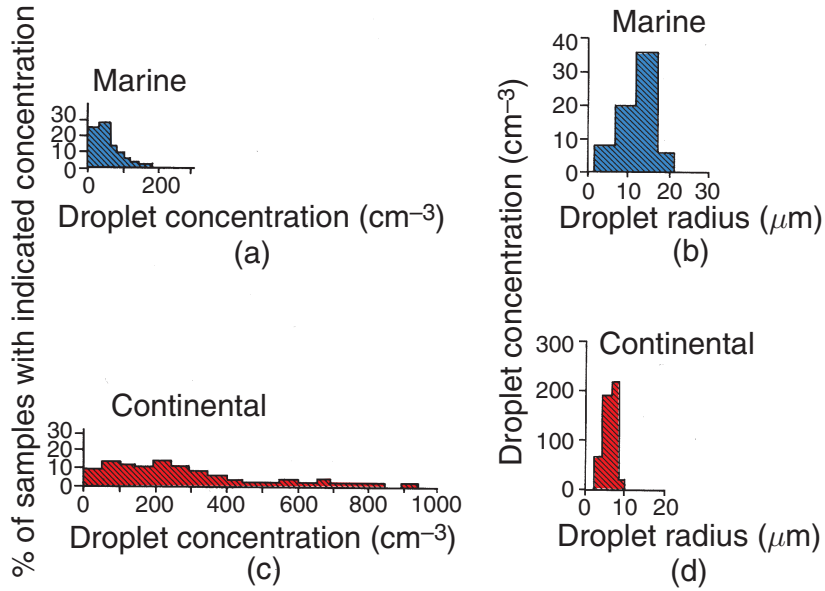

Fig. 6.7 (a) Percentage of marine cumulus clouds with indicated droplet concentrations. (b) Droplet size distributions in a marine cumulus cloud. (c) Percentage of continental cumulus clouds with indicated droplet concentrations. (d) Droplet size distributions in a continental cumulus cloud. Note change in ordinate from (b).

Coupled heat and mass transfer

Condensation/evaporation: equilibrium concentration at surface $c_s = c_s(T_s)$ is a function of temperature. When $T_s \neq T_\infty$ is unknown, solve coupled heat and mass transfer equation.

The latent heat released at the surface is balanced by the rates of heat conduction into the gas and particle surface.

$$\Delta_{vap} H (4\pi R_p^2) \tilde{J}_{A,r=R_p} = k \left(\frac{dT}{dr} \right)_{r=R_p} (4\pi R_p^2) + k_p \left(\frac{dT_p}{dr} \right)_{r=R_p} (4\pi R_p^2)$$

k and k_p are the thermal conductivies of the air and particle, respectively, and $\tilde{J}_{A,r} = -D_g(\partial c/\partial r)$.

Continuity equation for $Q = \rho c_p T$ (inernal heat energy per unit volume) $\Rightarrow$ neglect convection for dilute system (Stefan flow) $\Rightarrow$ steady-state heat transfer (Laplace equation) in 1-D:

$$\frac{d^2 T}{dr^2} + \frac{2}{r} \frac{dT}{dr} = 0$$

Solve subject to constraints:

$$T(R_p) = T_s$$

$$T(\infty) = T_\infty$$

Solution is

$$T(r) = T_\infty - \frac{R_p}{r} (T_\infty - T_s)$$

Steady-state solution to $c(r)$ is

$$c(r) = c_\infty - \frac{R_p}{r} (c_\infty - c_s)$$

Steady-state solution to energy balance:

$$T_s - T_\infty = \frac{\Delta_{vap} H D_g}{k} (c_\infty - c_s)$$

where $c_s = c_s(T_s)$.

The temperature at the surface will be higher than surrounding environment due to the latent heat released during condensation $(c_\infty - c_s)$.

Radiative broadening (broadening of size distribution) due to phenomena in larger droplets:

- loss of heat when $T_s > T_\infty$
- lowered saturation vapor pressure, more condensation
- proportional to surface area; dependent on ability for droplet to lose heat

When can the change in T_s be neglected? (approximately isothermal conditions)

- slowly evaporating species
- small heat of vaporization

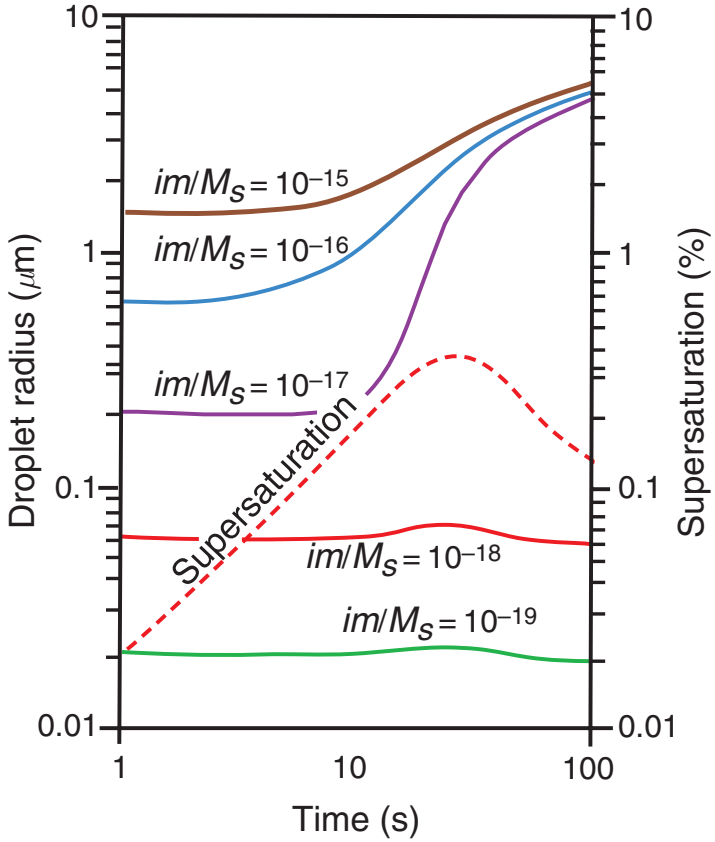

Fig. 6.16 Theoretical computations of the growth of cloud condensation nuclei by condensation in a parcel of air rising with a speed of 60 cm s^{-1}. A total of 500 CCN cm^{-1} was assumed with im/M_s values as indicated. Note how the droplets that have been activated (brown, blue, and purple curves) approach a monodispersed size distribution after just 100 s. The variation with time of the supersaturation of the air parcel is also shown (dashed red line).

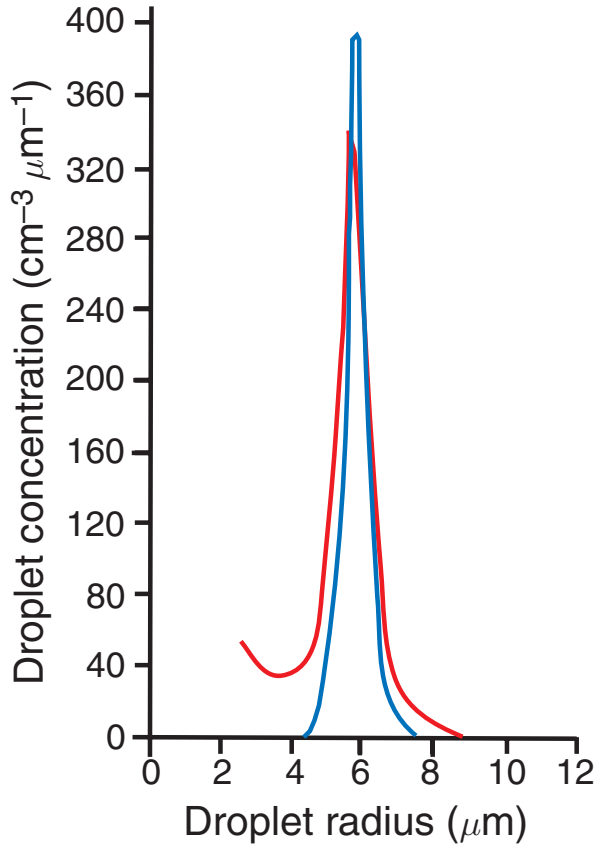

Fig. 6.17 Comparison of the cloud droplet size distribution measured 244 m above the base of a warm cumulus cloud (red line) and the corresponding computed droplet size distribution assuming growth by condensation only (blue line).

Cloud liquid water content (LWC)

in cumulus clouds

LWC:

- Adiabatic LWC = theoretical value of liquid water condensed when air parcel is lifted adiabatically
- True LWC is below adiabatic LWC because subsaturated air is entrained into cumulus clouds, primarily from top

Entrainment: Evaporation leads to cooling and loss of buoyancy $\rightarrow$ descent of air parcel $\rightarrow$ pockets of low LWC

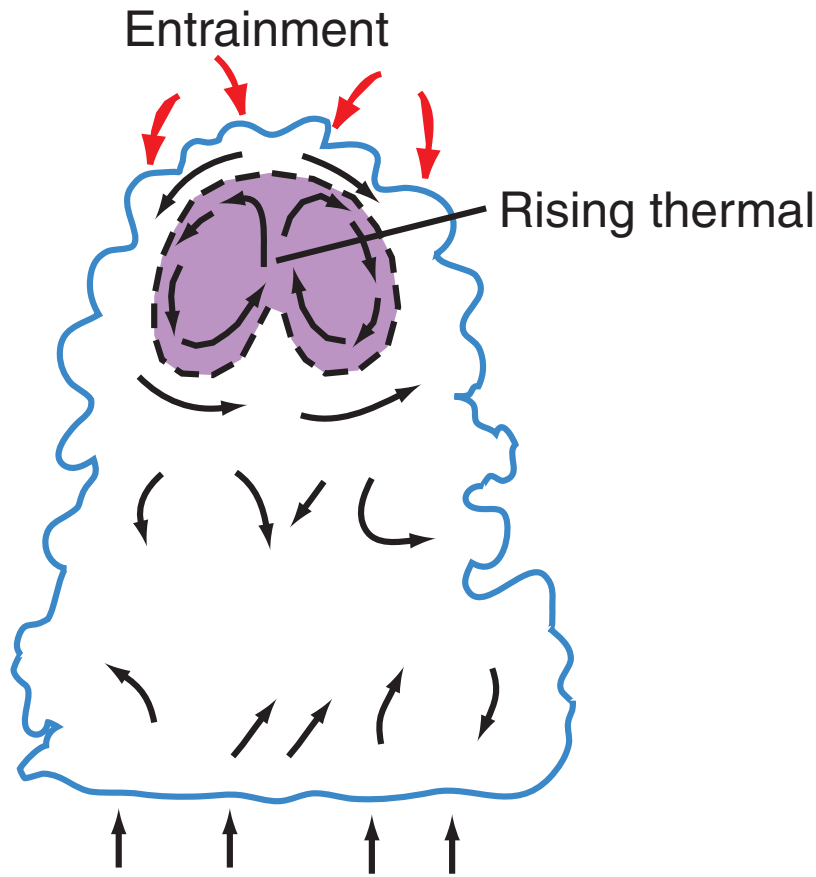

Fig. 6.12 Schematic of entrainment of ambient air into a small cumulus cloud. The thermal (shaded violet region) has ascended from cloud base.

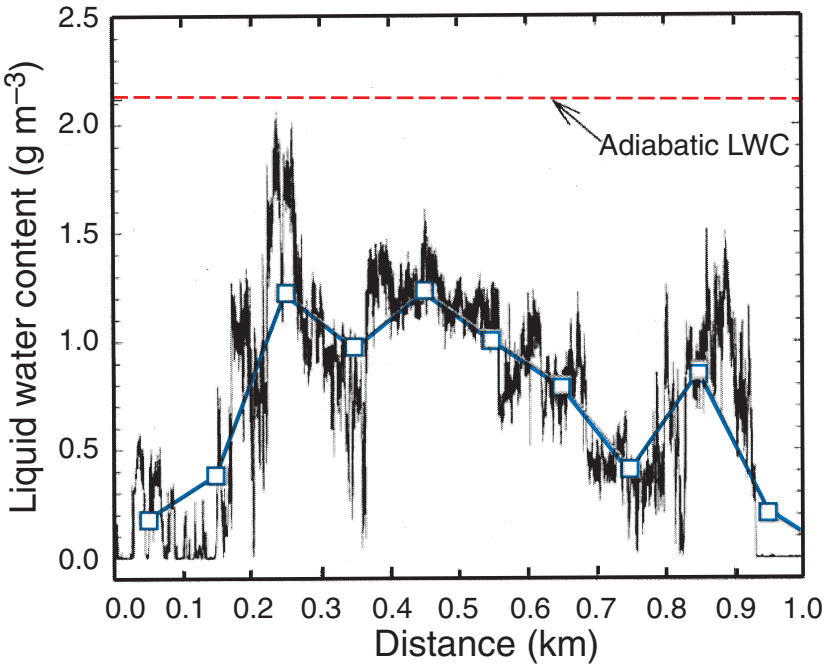

Fig. 6.10 High-resolution liquid water content (LWC) measurements (black line) derived from a horizontal pass through a small cumulus cloud. Note that a small portion of the cumulus cloud had nearly an adiabatic LWC. This feature disappears when the data are smoothed (blue line) to mimic the much lower sampling rates that were prevalent in older measurements.

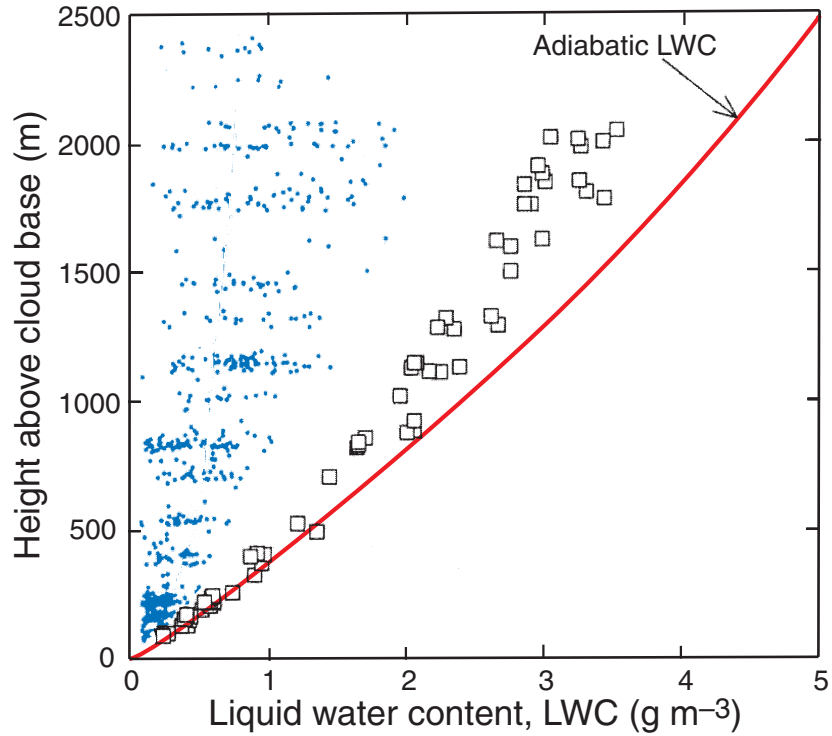

Fig. 6.11 Blue dots are average liquid water contents (LWC) measured in traverses of 802 cumulus clouds. Squares are the largest measured LWC. Note that no adiabatic LWC was measured beyond ∼900 m above the cloud base. Cloud base temperatures varied little for all flights, which permitted this summary to be constructed with a cloud base normalized to a height of 0 m.

Droplet growth mechanisms

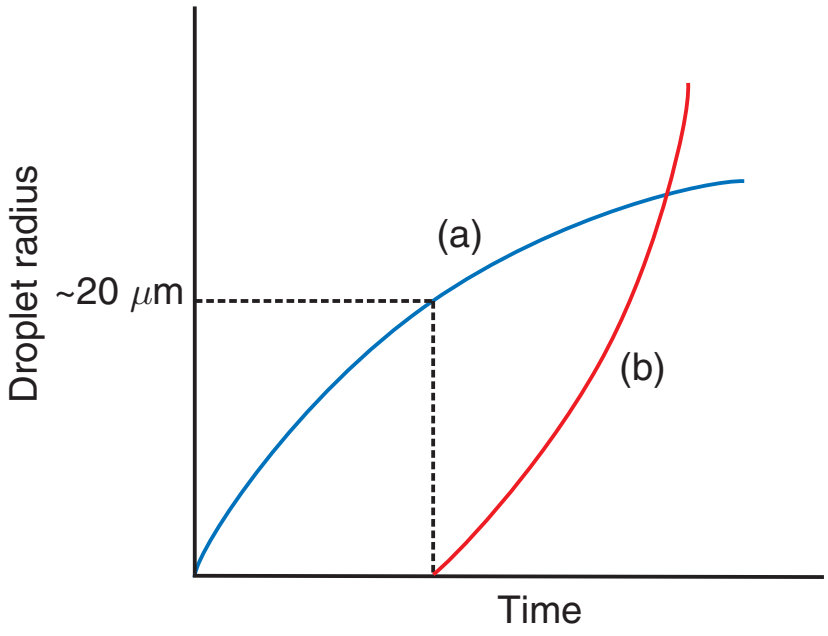

Fig. 6.15 Schematic curves of droplet growth (a) by condensation from the vapor phase (blue curve) and (b) by collection of droplets (red curve).

Droplet growth is rapid but does not permit enough growth $\rightarrow$ converges on a single size

Droplet collision-coalescence is slow but ultimately leads to largest droplets $\rightarrow$ leads to divergence in size and broadening of cloud droplet size distribution

Contrast with aerosol mechanisms

Condensation/evaporation modeling of water onto cloud droplets:

- $Kn \ll 1$; continuum regime (droplets are much larger than mean free path of gas)
- Consider effect of latent heat released during condensation on surface temperature

Droplet coalescence (coagulation between two liquid particles/droplets) :

- includes gravitational scavenging in addition to collision under turbulent conditions (rather than Brownian motion)
- also consider coalescence efficiency

Growth by condensation

Recall that we calculated the growth of an aerosol due to net condensation (molecular flux) for aerosols. The condensation of water vapor onto cloud droplet follows the same theory.

$$\frac{dM}{dt} = 4\pi r^2 D \frac{d\rho_v}{dr}$$

We can integrate between the equilibrium vapor density ρ_v (=concentration) at the droplet surface and bulk gas phase concentration (∞) uninfluenced by the droplet:

$$\frac{dM}{dt} \int_{r'=r}^{\infty} \frac{dr'}{r'^2} = 4\pi D \int_{\rho_v(r)}^{\rho_v(\infty)} d\rho_v$$

The solution can be written as

$$\frac{dM}{dt} = 4\pi r D[\rho_v(\infty) - \rho_v(r)]$$

or, as a function of droplet radius and water vapor pressure (recall relationship between pressure and concentration for an ideal gas):

$$\frac{dr}{dt} = \frac{1}{r} \frac{D\rho_v(\infty)}{\rho_l e(\infty)} [e(\infty) - e(r)]$$

ρ_l is the liqud water density.

Note that $e(r) = e'$, but $e(r) \approx e_s$ as $r \to \infty$ ($r > 1$ μm). If additionally, $e_s \approx e(\infty)$, the supersaturation is approximated as

$$\frac{e(\infty) - e(r)}{e(\infty)} \approx \frac{e(\infty) - e_s}{e_s} = S$$

We can rewrite the growth equation as

$$r\frac{dr}{dt} = G_l S$$

where G_l is a term that has a constant value for a given environment.

$$G_l = \frac{D\rho_v(\infty)}{\rho_l}$$

Terminal velocity of a cloud droplet

gravitational settling/sedimentation

Deriving the terminal velocity for a spherical particle/droplet:

$$F_{\text{drag}} = (\rho_p V_p - \rho_{\text{air}} V_{\text{air}})$$

For a droplet of radius R_p,

$$F_{\text{drag}} = \frac{4}{3}\pi R_p^3 g \left(\rho_{\text{air}} - \rho_p\right)$$

For spheres with $R_p \leq 20\mu$m, Stokes' drag force is

$$F_{\text{drag}} = 6\pi\mu R_p v_t$$

where v_t is the terminal velocity of the particle, which can be written (for $\rho_p \gg \rho_{\text{air}}$) as

$$v_t = \frac{2}{9}\frac{R_p^2\left(\rho_p - \rho_{\text{air}}\right)g}{\mu} \approx \frac{2}{9}\frac{R_p^2 \rho_p g}{\mu}$$

As the droplet increases in size ($\geq 20\mu$m), becomes increasingly nonspherical and leaves an increasing wake $\rightarrow$ larger drag force than given here.

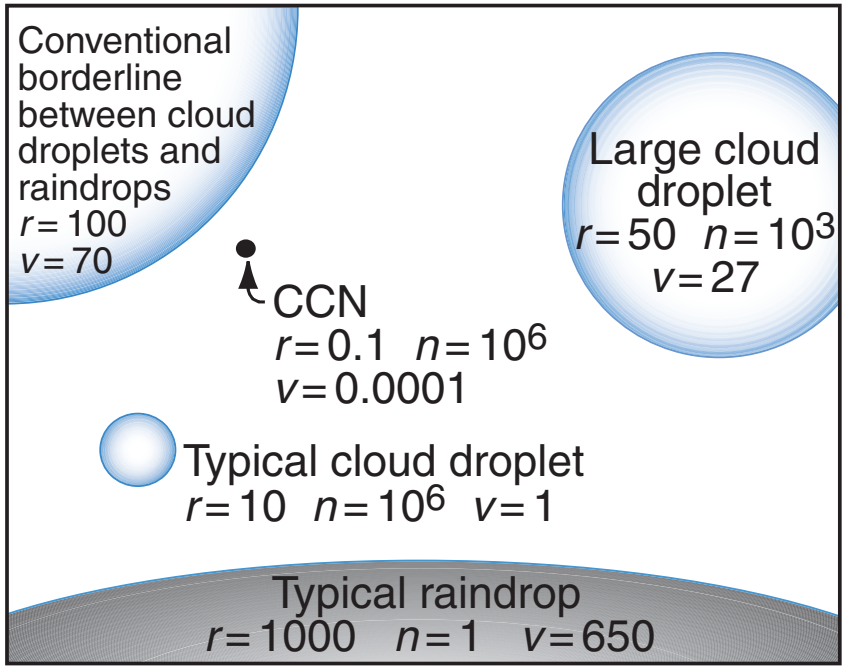

Fig. 6.18 Relative sizes of cloud droplets and raindrops; r is the radius in micrometers, n is the number per liter of air, and v is the terminal fall speed in centimeters per second. The circumferences of the circles are drawn approximately to scale, but the black dot representing a typical CCN is 25 times larger than it should be relative to the other circles.

Flattening of settling velocities due to nonsphericity

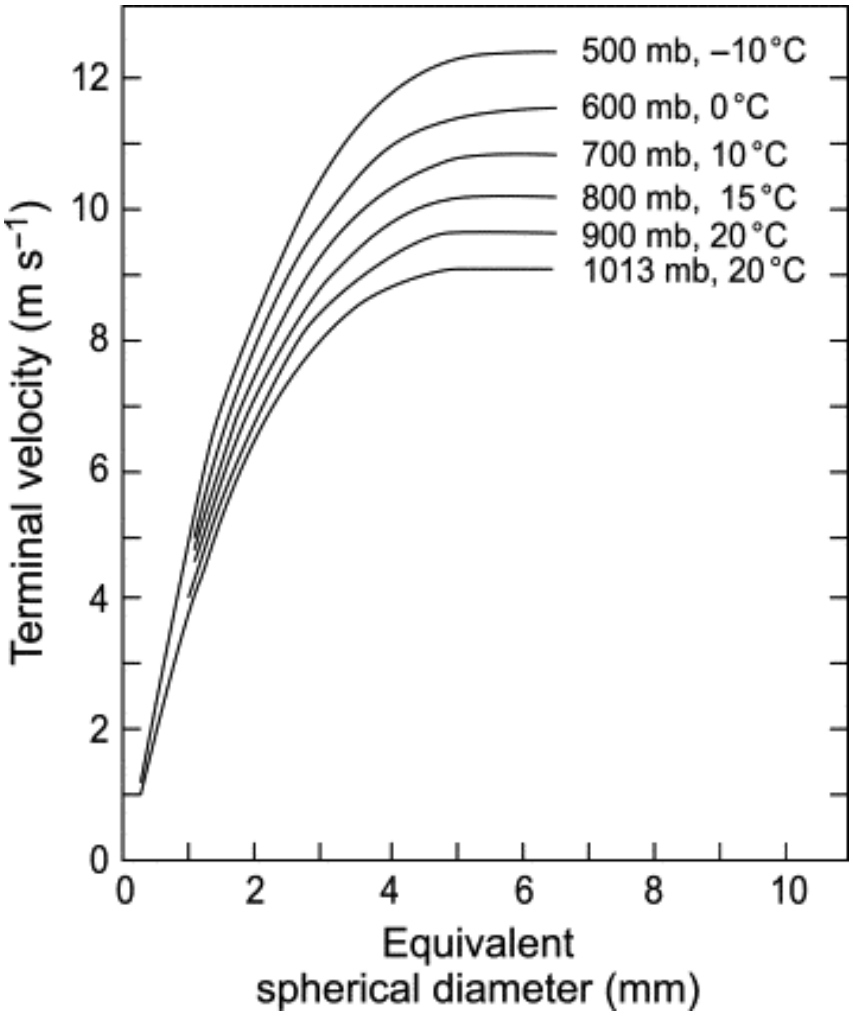

Houze, 2014

Differential settling velocities leads to collision

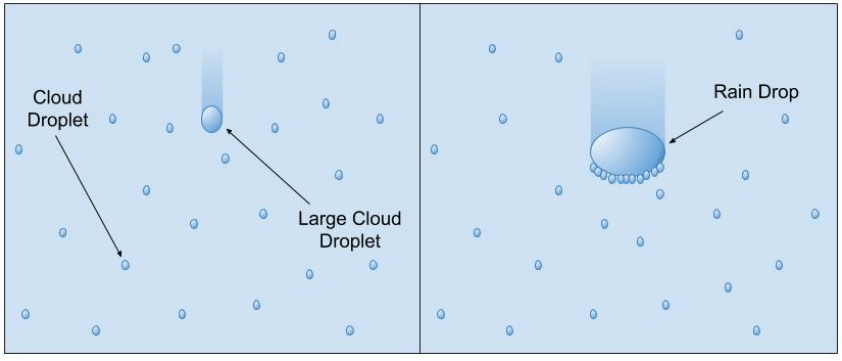

Nugent et al.

Collision efficiency

Here we switch notation from R_p to r to indicate droplet radius.

For a droplet of radius r_1 overtaking a smaller droplet of radius r_2 with effective cross section of y, the collision efficiency E is

$$E = \frac{\pi y^2}{\pi (r_1 + r_2)^2} = \frac{y^2}{(r_1 + r_2)^2}$$

- $r_2/r_1 \ll 1$, smaller droplets follow streamlines around the collector drop
- $0.6 < r_2/r_1 < 0.9$, $v_{t,1} \sim v_{t,2}$ so E falls off
- $r_2/r_1 \to 1$, two nearly equal sized drops interact strongly

Note that wake effects can produce values of E greater than unity.

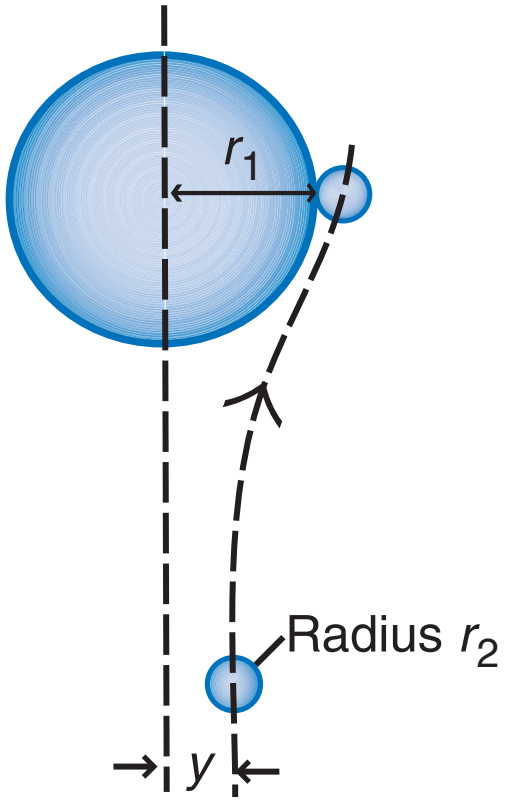

Fig. 6.19 Relative motion of a small droplet with respect to a collector drop. y is the maximum impact parameter for a droplet of radius r_2 with a collector drop of radius r_1.

Coalescence efficiency

It is known from laboratory experiments that droplets can bounce off one another or off a plane surface of water. We introduce another coefficient, E', which considers whether a droplet is captured when it collides with a larger drop.

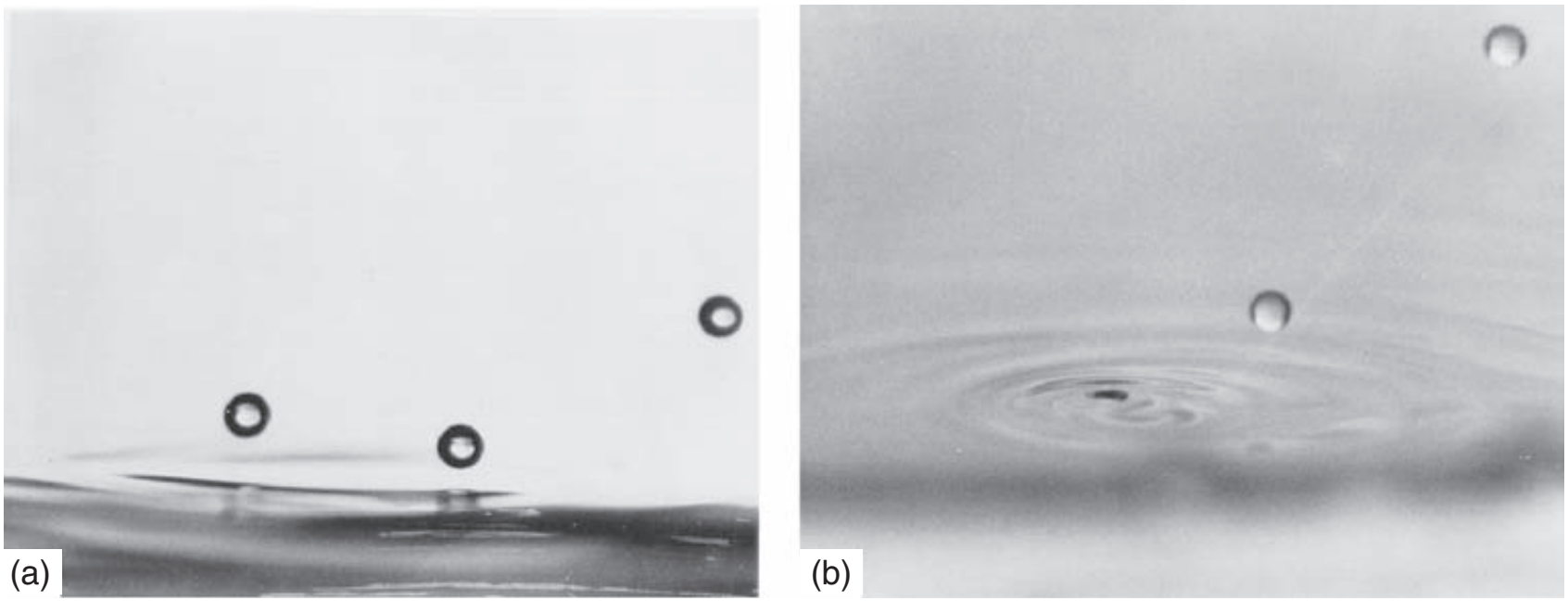

Fig. 6.21 (a) A stream of water droplets (entering from the right), about 100 μm in diameter, rebounding from a plane surface of water. (b) When the angle between the stream of droplets and the surface of the water is increased beyond a critical value, the droplets coalesce with the water.

Collection efficiency

The collection efficiency E_c between two droplets is a product of the collision efficiency E and the coalescence efficiency E':

$$E_c = EE'$$

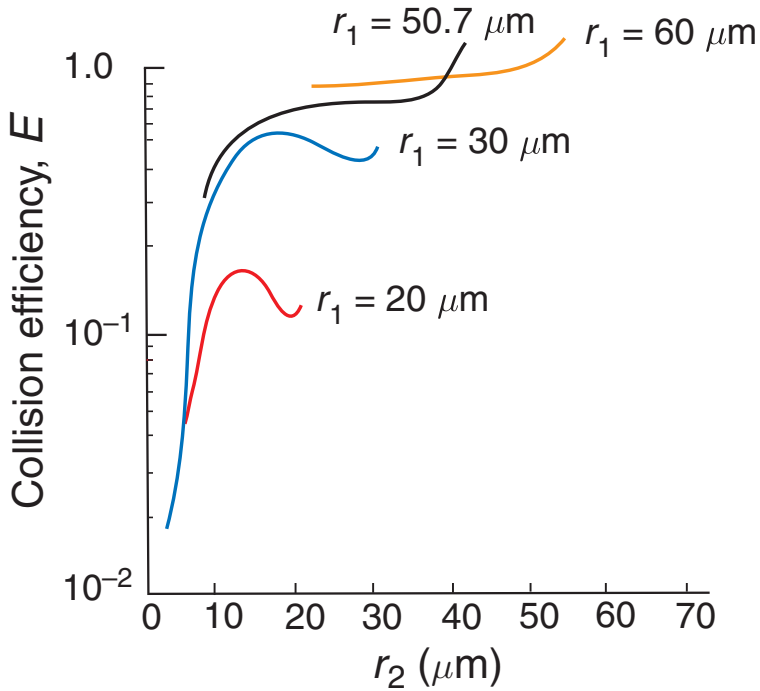

Fig. 6.20 Calculated values of the collision efficiency, E, for collector drops of radius r_1 with droplets of radius r_2.

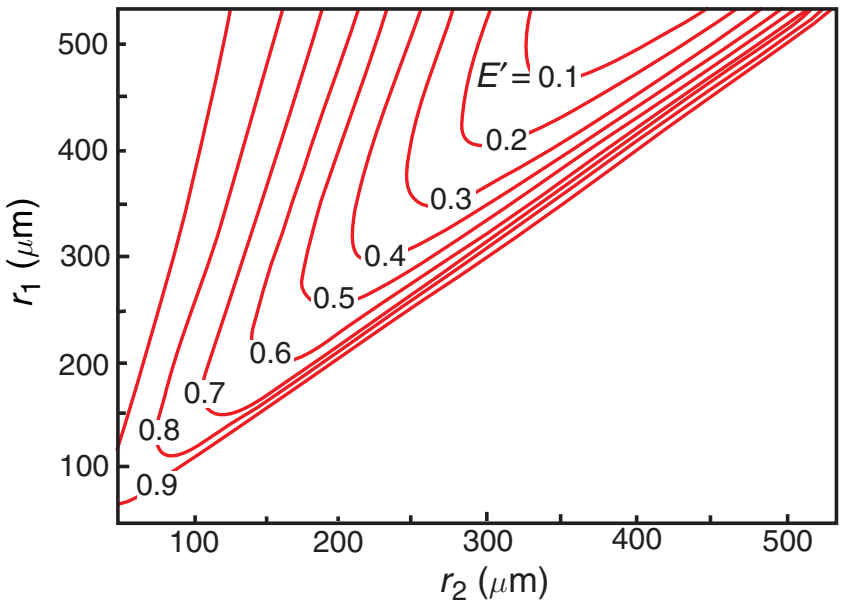

Fig. 6.22 Coalescence efficiencies E for droplets of radius r_2 with collector drops of radius r_1 based on an empirical fit to laboratory measurements.

Continuous collection model

Change in droplet mass M with time as two droplets (denoted as 1 and 2) collide:

$$\frac{dM}{dt} = \pi r_1^2 (v_1 - v_2) w_l E_c$$

$$\text{where} \quad M = \frac{4}{3}\pi r_1^3 \rho_l$$

w_l is the liquid water content of droplets with r_2 and ρ_l is the liquid water density. If $v_1 \gg v_2$ and $E' \approx 1$ ($E_c = E$),

$$\frac{dr_1}{dt} = \frac{v_1 w_l E}{4\rho_l}$$

For steady updraft velocity w,

$$\frac{dz}{dt} = w - v_1$$

Change radius as function of height

$$\frac{dr_1}{dz} = \frac{v_1 w_l E}{4\rho_l (w - v_1)}$$

Efficient collectors $\geq$ 20 μm in deep clouds $\rightarrow \sim$1 h for growth to raindrops.

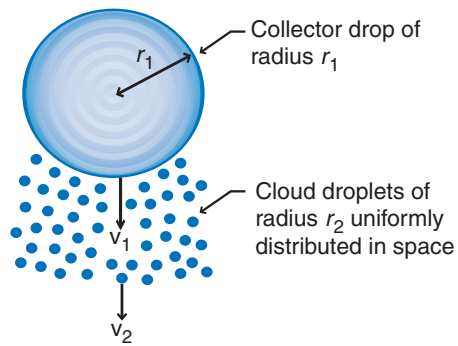

Fig. 6.23 Schematic illustrating the continuous collection model for the growth of a cloud drop by collisions and coalescence.

How can efficent collectors be formed from approximately monodisperse droplets $\sim$10 μm?

How do broad cloud droplet sizes result?

Proposed mechanisms:

- Giant CCN (large collector drops)
- Effects of turbulence and inhomogeneities
- Radiative broadening (enhancement of water uptake by larger particles)
- Stochastic collection (Fig. 6.24))

Higher CCN concentrations over continent $\rightarrow$ less likely to rain (Fig. 6.25)

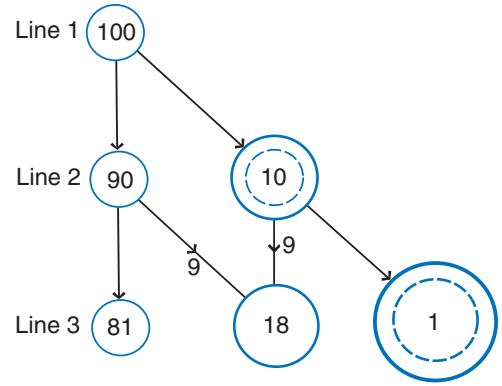

Fig. 6.24 Schematic diagram to illustrate broadening of droplet sizes by statistical collisions.

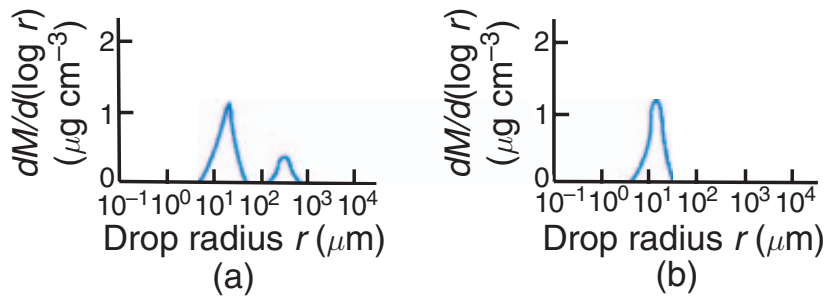

Fig. 6.25 Numerical predictions of the mass spectrum of drops near the middle of (a) a warm marine cumulus cloud and (b) a warm continental cloud after 67 min of growth.

Breakup and raindrop size distributions

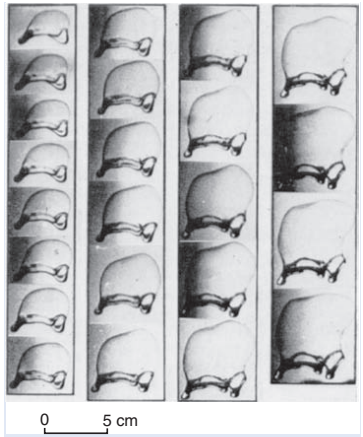

Fig. 6.26 Sequence of high-speed photographs (starting at upper left and moving down and to the right) showing how a large drop in free fall forms a parachutelike shape with a toroidal ring of water around its lower rim. The toroidal ring becomes distorted and develops cusps separated by threads of water. The cusps eventually break away to form large drops, and the thin film of water that forms the upper part of the parachute bursts to produce a spray of small droplets. Time interval between photographs = 1 ms. [Photograph courtesy of B. J. Mason.]

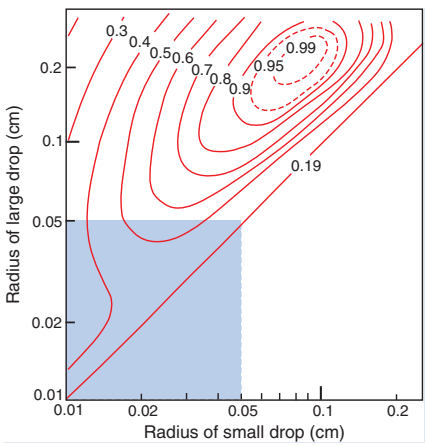

Fig. 6.28 Empirical results for the probability of breakup (expressed as a fraction and shown on the contours) following the collision and initial coalescence of two drops. The shaded region is covered by Fig. 6.21, but note that Fig. 6.21 shows the probability of coalescence rather than breakup. [Based on J. Atmos. Sci. 39, 1600 (1982).]

Due to breakup, maximum raindrop radius $\sim$5 mm.

Breakup mechamisms:

- inverted bag and bursting
- droplet collisions

Marshall-Palmer distribution:

$$n_N(r_r) = N_0 \exp(-\Gamma r_r)$$

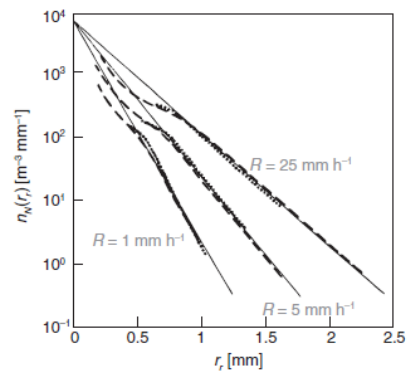

Fig. 9.1 Measured raindrop size distributions $n_N(r_r)$ (broken and dotted lines) for different rain rates R as a function of the radius of the raindrops r_r, together with best fit exponential curves (solid lines). Figure adapted from Marshall and Palmer (1948) with permission of the American Meteorological Society.

Lohmann et al., 2016

Heterogeneous and multi-phase chemistry

Aqueous-phase chemistry (including gas-particle partitioning): warm cloud droplets

Reactions on solid surfaces: surfaces of ice (and particles)

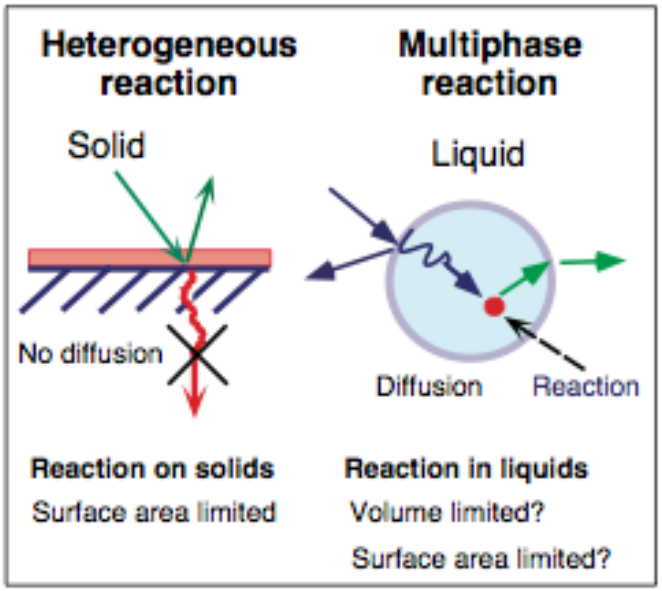

Fig. 1. Distinction between heterogeneous and multiphase reactions. The slab on the solid is meant to represent a quasi-liquid layer, if it is present. Diffusion into and out of the bulk of the solid is assumed to be too slow to effect the concentrations at the surface; thus, the reaction is confined to the surface. In the case of the liquid, it is assumed that the reaction takes place after the molecule has been incorporated into the bulk of the liquid.

Ravishankara, 1997

Warm cloud (aqueous-phase) chemistry

Liquid droplets in warm clouds are mini-reactors

Many reactions initiated by dissolution of gases

Net result of aqueous-phase chemistry:

- evaporated cloud droplets leave aerosols which contain reacted products and dissolved (water-soluble) gases in concentrated form (gas/particle conversion)
- over half of global sulfate aerosol production is due to this process
- uptake of acidic gases leads to acid precipitation

Cloud liquid water content is orders of magnitude greater than aerosol liquid water content.

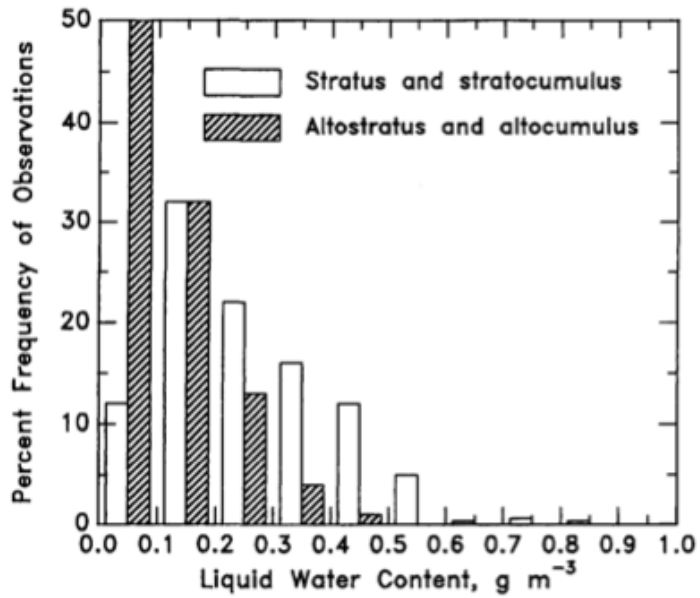

FIGURE 7.2 Frequency distribution for liquid water content average values for various cloud types over Europe and Asia.

Seinfeld and Pandis, 2006

Evaporation of cloud droplets lead to aerosols which participate in additional microphysical processes

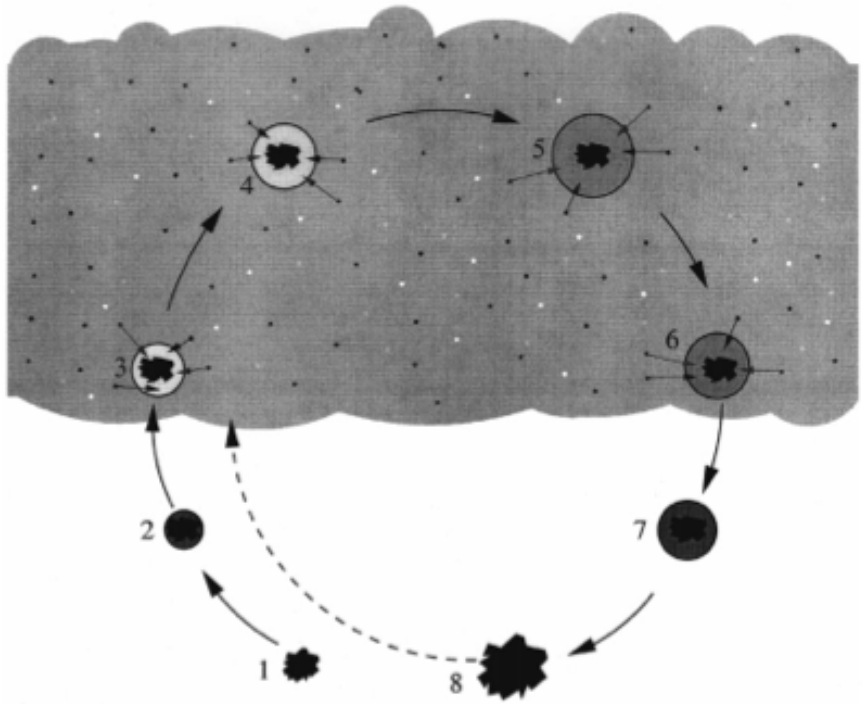

Fig. 1. Schematic illustration of the aerosol-cloud-cycling process. For a description of the different stages, see text.

Bott, 1999

1. dry particle
2. wet particle
3. cloud droplet
4. cloud droplet with increasing amount of dissolved gases
5. cloud droplet with increasing amount of dissolved gases
6. cloud droplet with increasing amount of dissolved gases
7. particle concentrated in dissolved water-soluble substances
8. dry aerosol particle with increased water soluble mass fraction

Oxidation of SO_2 [S(IV)] to SO_4^{2-} [S(VI)]

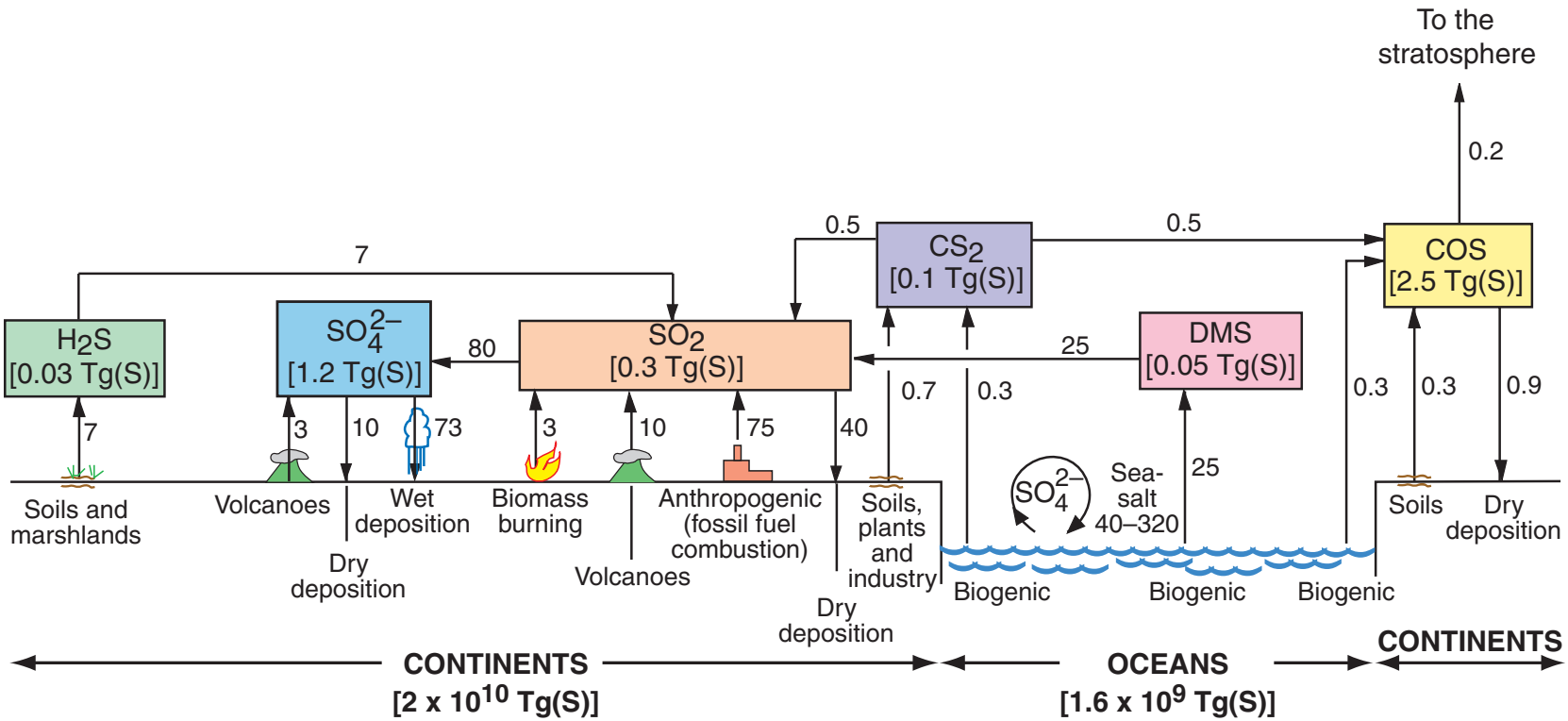

Fig. 5.15 Numbers alongside the arrows are estimates of average annual fluxes in Tg(S) per year; various degrees of uncertainty, some quite large, are associated with all of the fluxes. Numbers in square brackets are total amounts of the species in the atmosphere. For clarity, wet and dry removal are shown only over the continents, although they also occur over the oceans.

Mass transfer and acid-base equilibria

Dissolution of gases is followed by aqueous-phase chemistry.

To consider dissolution of gases into cloud liquid water, we have to consider

- gas-phase diffusion
- surface uptake
- solvation/reaction

Timescales of mass transfer are on the order of milliseconds to a second—*can assume equilibrium governed by Henry's law in many cases*.

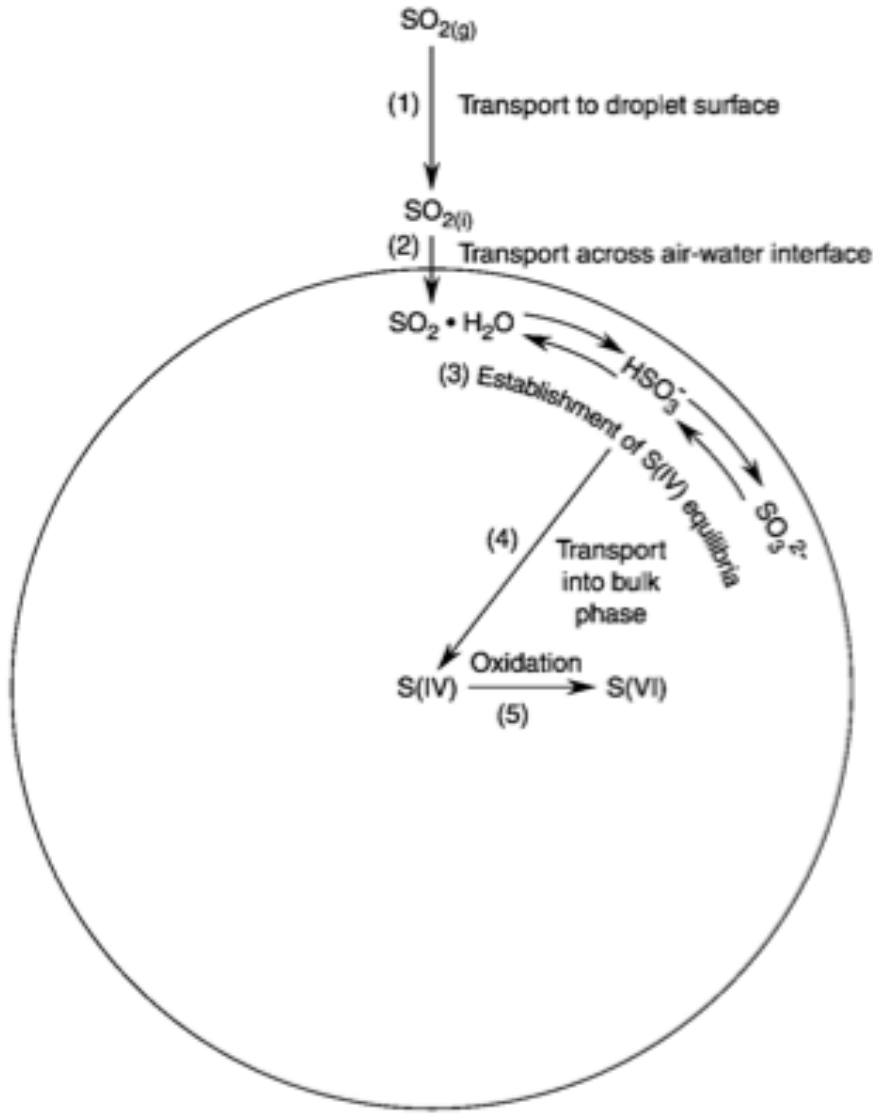

FIGURE 8.11 Schematic of steps involved in the transfer of SO_2 from the gas phase to the aqueous phase of an atmospheric water droplet and its oxidation in the liquid phase. $SO_{2(l)} = SO_2$ at the water–gas interface.

Finlayson-Pitts and Pitts, 1999

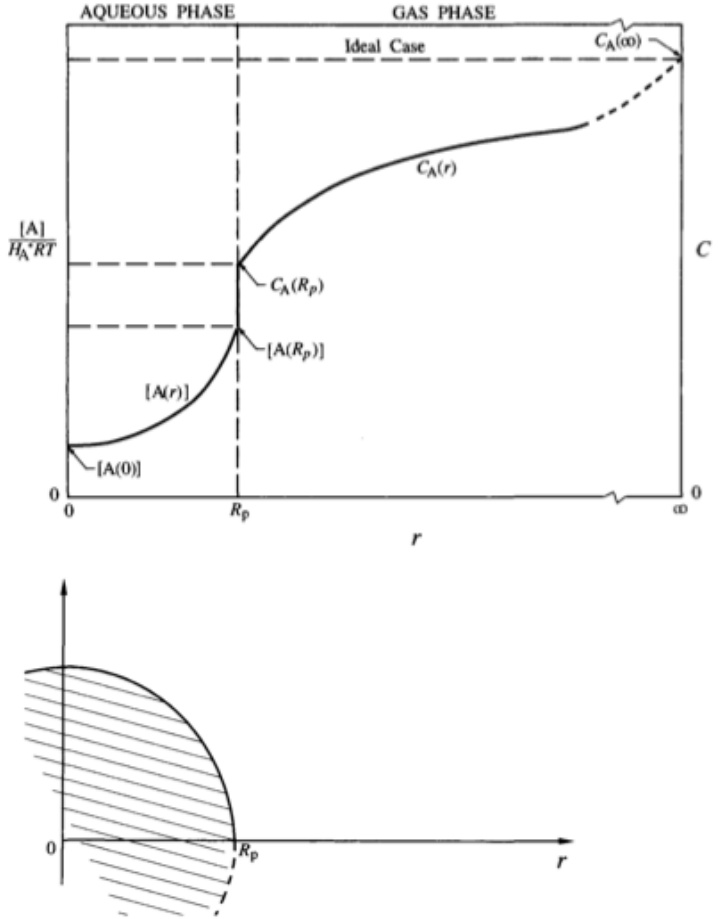

FIGURE 12.5 Schematic of gas- and aqueous-phase steady-state concentration profiles for the case where there are gas-phase, interfacial, and aqueous-phase mass transport limitations. Also shown is the ideal case where there are no mass transport limitations.

Seinfeld and Pandis, 2006

Dissolution of gases in cloud liquid water

TABLE 7.2 Henry's Law Coefficients of Some Atmospheric Gases

Species[a]	H(M atm^{-1}) at 298 K
O_2	1.3×10^{-3}
NO	1.9×10^{-3}
C_2H_4	4.8×10^{-3}
NO_2	1.0×10^{-2}
O_3	1.1×10^{-2}
N_2O	2.5×10^{-2}
CO_2	3.4×10^{-2}
H_2S	0.1
DMS	0.56
HCl	1.1
SO_2	1.23
NO_3	1.8
CH_3ONO_2	2.0
CH_3O_2	6
OH	25
HNO_2	49
NH_3	62
CH_3OH	220
CH_3OOH	310
$CH_3C(O)OOH$	473
HO_2	5.7×10^3
HCOOH	3.6×10^3
HCHO[b]	2.5
CH_3COOH	8.8×10^3
H_2O_2	1×10^5
HNO_3	2.1×10^5

[a] The values given reflect only the physical solubility of the gas regardless of the subsequent fate of the dissolved species. These constants do not account for dissociation or other aqueous-phase transformations.

[b] The value is 6.3×10^3 if the diol formation is included.

One form of Henry's law:

$$[i] = H_i p_i$$

H_i is the Henry's law constant; p_i is in units of atm and $[i]$ is the solution-phase concentration of i in units of molarity (M; mole L^{-1}).

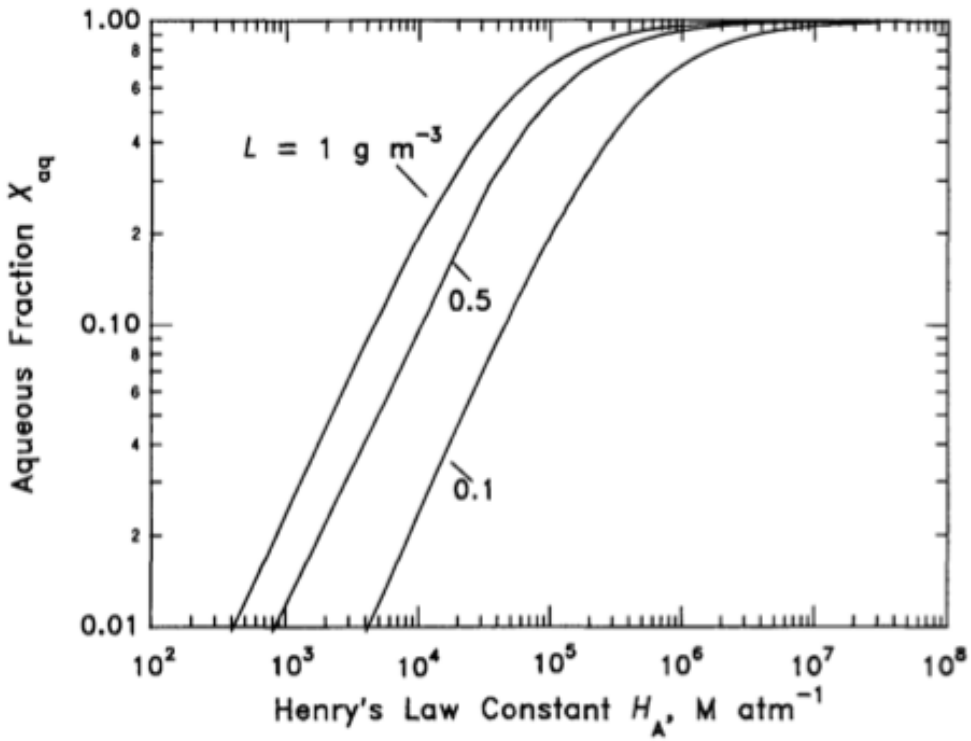

FIGURE 7.3 Aqueous fraction of a species as a function of the cloud liquid water content and the species' Henry's law constant.

Seinfeld and Pandis, 2006

Carbon dioxide-water equilibrium

Stoichiometric balance:

$$CO_{2(g)} + H_2O \rightleftharpoons CO_2 \cdot H_2O$$

$$CO_2 \cdot H_2O \rightleftharpoons H^+ + HCO_3^-$$

$$HCO_3^- \rightleftharpoons H^+ + CO_3^{2-}$$

Mass law expressions:

$$K_{hc} = H_{CO_2} = \frac{[CO_2 \cdot H_2O]}{p_{CO_2}}$$

$$K_{c1} = \frac{[H^+][HCO_3^-]}{[CO_2 \cdot H_2O]}$$

$$K_{c2} = \frac{[H^+][CO_3^{2-}]}{[HCO_3^-]}$$

Concentrations:

$$[CO_2 \cdot H_2O] = H_{CO_2} p_{CO_2}$$

$$[HCO_3^-] = \frac{K_{c1}[CO_2 \cdot H_2O]}{[H^+]} = \frac{H_{CO_2} K_{c1} p_{CO_2}}{[H^+]}$$

$$[CO_3^{2-}] = \frac{K_{c2}[HCO_3^-]}{[H^+]} = \frac{H_{CO_2} K_{c1} K_{c2} p_{CO_2}}{[H^+]^2}$$

Total concentration:

$$[CO_2^T] = [CO_2 \cdot H_2O] + [HCO_3^-] + [CO_3^{2-}]$$

$$= H_{CO_2} p_{CO_2} \left(1 + \frac{K_{c1}}{[H^+]} + \frac{K_{c1} K_{c2}}{[H^+]^2}\right)$$

Effective Henry's law constant:

$$H^*_{CO_2} = H_{CO_2} \left(\frac{K_{c1}}{[H^+]} + \frac{K_{c1} K_{c2}}{[H^+]^2}\right)$$

Note that

$$H^*_{CO_2} > H_{CO_2}$$

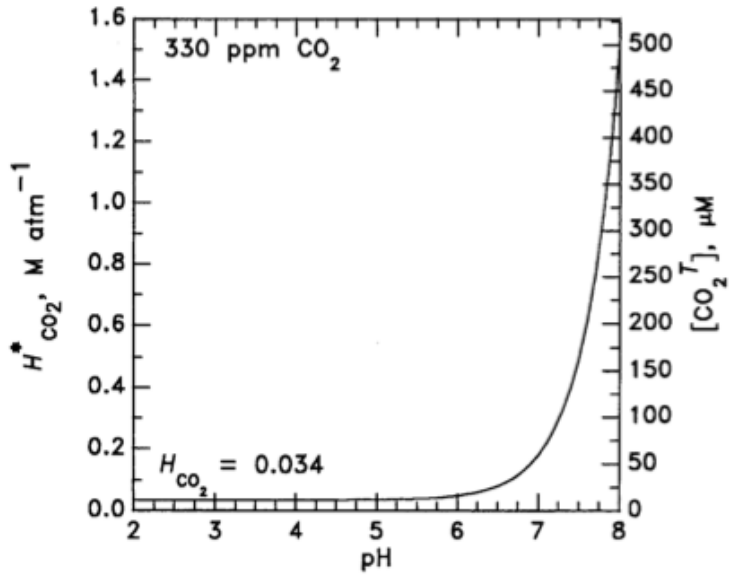

FIGURE 7.4 Effective Henry's law constant for CO_2 as a function of the solution pH. Also shown is the corresponding equilibrium total dissolved CO_2 concentration $[CO_2^T]$ for a CO_2 mixing ratio of 330 ppm.

Seinfeld and Pandis, 2006

Example: pH of "pure" rainwater

For a system containing only CO_2 with mixing ratio of ξ_{CO_2} = 350 ppm and water at 298 K, what is the pH of cloudwater and rain droplets in this system (assume equilibrium between gas and condensed phase)?

Charge balance

$$[H^+] = [OH^-] + [HCO_3{}^-] + 2[CO_3{}^{2-}]$$

Replace concentrations with mass law relations:

$$[H^+] = \frac{K_w}{[H^+]} + \frac{H_{CO_2} K_{c1} p_{CO_2}}{[H^+]} + \frac{H_{CO_2} K_{c1} K_{c2} p_{CO_2}}{[H^+]^2}$$

Rearrange as a cubic equation,

$$[H^+]^3 - \left(K_w + H_{CO_2} K_{c1} p_{CO_2}\right)[H^+] - 2 H_{CO_2} K_{c1} K_{c2} p_{CO_2} = 0$$

$\Rightarrow$ *The solution pH is 5.6.*

TABLE 7.4 Thermodynamic Data for Aqueous Equilibrium Constants

Equilibrium	K at 298 K (M)	ΔH_A at 298 K, kcal mol^{-1}
$H_2O \rightleftharpoons H^+ + OH^-$	1.0×10^{-14}	13.35
$CO_2 \cdot H_2O \rightleftharpoons H^+ + HCO_3^-$	4.3×10^{-7}	1.83
$HCO_3^- \rightleftharpoons H^+ + CO_3^{2-}$	4.7×10^{-11}	3.55
$SO_2 \cdot H_2O \rightleftharpoons H^+ + HSO_3^-$	1.3×10^{-2}	−4.16
$HSO_3^- \rightleftharpoons H^+ + SO_3^{2-}$	6.6×10^{-8}	−2.23
$NH_3 \cdot H_2O \rightleftharpoons NH_4^+ + OH^-$	1.7×10^{-5}	8.65

$$p_{CO_2} = 350 \times 10^{-9} \text{ atm}$$
$$H_{CO_2} = 3.4 \times 10^{-2} \text{ M atm}^{-1}$$
$$K_{c1} = 4.3 \times 10^{-7} \text{ M}$$
$$K_{c2} = 4.7 \times 10^{-11} \text{ M}$$
$$K_w = 10^{-14} \text{ M}$$

Aqueous-phase uptake of SO_2 and partitioning of S(IV) species

Stoichiometric balance

$$SO_{2(g)} + H_2O \rightleftharpoons SO_2 \cdot H_2O$$

$$SO_2 \cdot H_2O \rightleftharpoons H^+ + HSO_3^-$$

$$HSO_3^- \rightleftharpoons H^+ + SO_3^{2-}$$

Mass law expressions

$$H_{SO_2} = \frac{[SO_2 \cdot H_2O]}{p_{SO_2}} = 1.242\ \mathrm{M\,atm^{-1}}$$

$$K_{s1} = \frac{[H^+][HSO_3^-]}{[SO_2 \cdot H_2O]} = 1.32 \times 10^{-2}\ \mathrm{M}$$

$$K_{s2} = \frac{[H^+][SO_3^-]}{[HSO_3^-]} = 6.42 \times 10^{-8}\ \mathrm{M}$$

Concentrations

$$[SO_2 \cdot H_2O] = H_{SO_2} p_{SO_2}$$

$$[HSO_3^-] = \frac{K_{s1}[SO_2 \cdot H_2O]}{[H^+]} = \frac{H_{SO_2} K_{s1} p_{SO_2}}{[H^+]}$$

$$[SO_3^{2-}] = \frac{K_{s2}[HSO{-}3]}{[H^+]} = \frac{H_{SO_2} K_{s1} K_{s2} p_{SO_2}}{[H^+]^2}$$

Mass balance:

$$[S(IV)] = [SO_2 \cdot H_2O] + [HSO_3^-] + [SO_3^{2-}]$$

Total concentration

$$[S(IV)] = H_{SO_2} p_{SO_2} \left[1 + \frac{K_{s1}}{[H^+]} + \frac{K_{s1} K_{s2}}{[H^+]^2}\right]$$

$$= H^*_{S(IV)} p_{SO_2}$$

Effective Henry's law constant

$$H^*_{S(IV)} = H_{SO_2} \left[1 + \frac{K_{s1}}{[H^+]} + \frac{K_{s1} K_{s2}}{[H^+]^2}\right]$$

Mole fractions

$$x_{SO_2 \cdot H_2O} = \frac{[SO_2 \cdot H_2O]}{[S(IV)]} = \left(1 + \frac{K_{s1}}{[H^+]} + \frac{K_{s1} K_{s2}}{[H^+]}\right)^{-1}$$

$$x_{HSO_3} = \frac{[HSO_3^-]}{[S(IV)]} = \left(1 + \frac{[H^+]}{K_{s1}} + \frac{K_{s2}}{[H^+]}\right)^{-1}$$

$$x_{SO_3^{2-}} = \frac{[SO_{32}^-]}{[S(IV)]} = \left(1 + \frac{[H^+]}{K_{s2}} + \frac{[H^+]^2}{K_{s1} K_{s2}}\right)^{-1}$$

Dissolution of SO_2

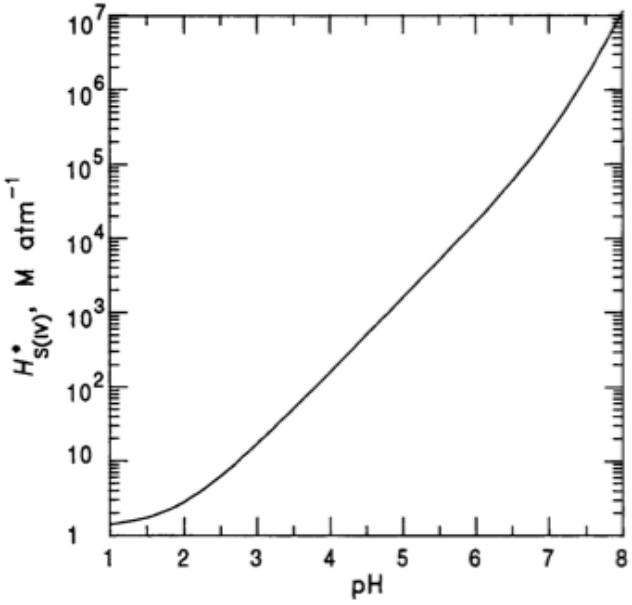

FIGURE 7.6 Effective Henry's law constant for SO_2 as a function of solution pH at 298 K.

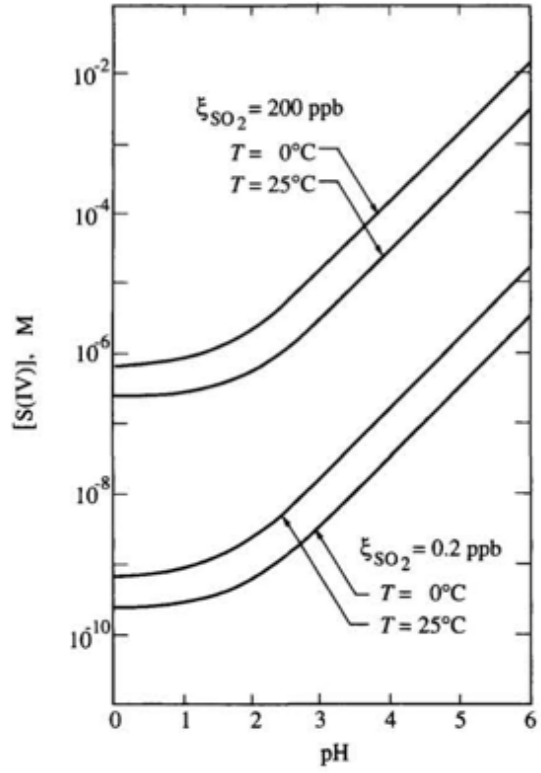

FIGURE 7.7 Equilibrium dissolved S(IV) as a function of pH, gas-phase mixing ratio of SO_2, and temperature.

Seinfeld and Pandis, 2006

Partitioning of S(IV) species

Partitioning of S(IV) species

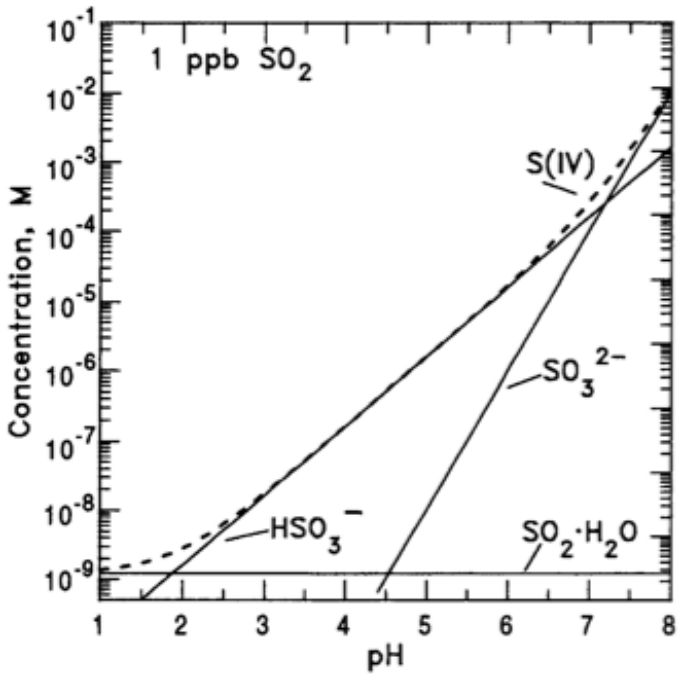

FIGURE 7.5 Concentrations of S(IV) species and total S(IV) as a function of solution pH for an SO_2 mixing ratio of 1 ppb at 298 K.

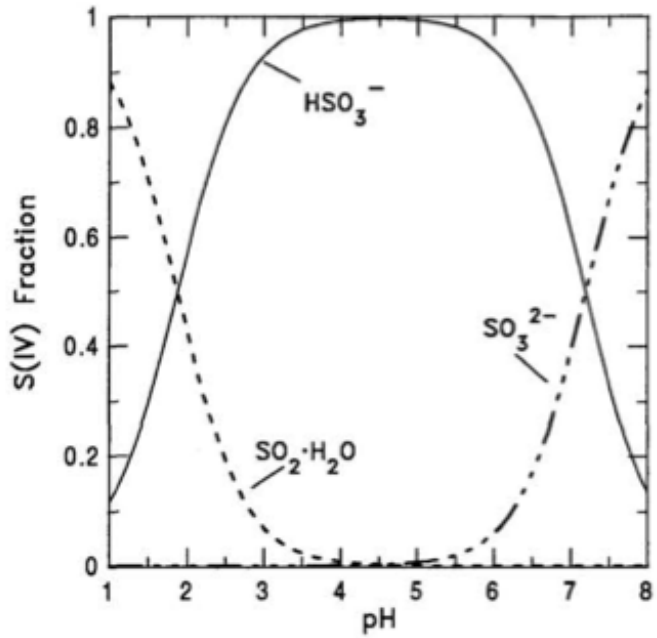

FIGURE 7.8 Concentrations of S(IV) species expressed as S(IV) mole fractions. These fractions are independent of the gas-phase SO_2 concentration.

Seinfeld and Pandis, 2006

Oxidation of S(IV) and S(VI) (sulfate) formation

Reaction of S(IV) with dissolved species $A_{(aq)}$

$$S(IV) + A_{(aq)} \rightarrow \text{products}$$

for which the rate of reaction is generally given by

$$R_a = \frac{-dS(IV)}{dt} = k[A_{(aq)}][S(IV)] \quad \mathrm{M\,s^{-1}}$$

Mechanisms of oxidation:

- by dissolved O_3

$$S(IV) + O_3 \rightarrow S(VI) + O_2$$

- by hydrogen peroxide:
  nucleophilic displacement by hydrogen peroxide on bisulfite

$$HSO_3^- + H_2O_2 \rightleftharpoons SO_2OOH^- + H_2O$$

  followed by protoantion of peroxymonosulfurous acid

$$SO_2OOH^- + H^+ \rightarrow H_2SO_4$$

- by O_2 catalyzed by iron and manganese

$$S(IV) + \frac{1}{2}O_2 \xrightarrow{Mn^{2+},Fe^{3+}} S(VI)$$

Oxidation pathways of S(IV) $\rightarrow$ S(VI)

S(IV) can additionally be oxidized by natural transition metal elements (e.g., present in mineral dust aerosol).

TABLE 7.6 Rate Expressions for Sulfate Formation in Aqueous Solution Used in Computing Figure 7.19

Oxidant	Rate Expression, $-d[S(IV)]/dt$	Reference
O_3	$(k_0[SO_2 \cdot H_2O] + k_1[HSO_3^-] + k_2[SO_3^{2-}])[O_3(aq)]$	Hoffmann and Calvert (1985)
	$k_0 = 2.4 \times 10^4\ M^{-1}\ s^{-1}$	
	$k_1 = 3.7 \times 10^5\ M^{-1}\ s^{-1}$	
	$k_2 = 1.5 \times 10^9\ M^{-1}\ s^{-1}$	
H_2O_2	$k_4[H^+][HSO_3^-][H_2O_2(aq)]/(1 + K[H^+])$	Hoffmann and Calvert (1985)
	$k_4 = 7.45 \times 10^7\ M^{-1}\ s^{-1}$	
	$K = 13\ M^{-1}$	
Fe(III)	$k_5[Fe(III)][SO_3^{2-}]^a$	Hoffmann and Calvert (1985)
	$k_5 = 1.2 \times 10^6\ M^{-1}\ s^{-1}$ for pH ≤ 5	
Mn(II)	$k_6[Mn(II)][S(IV)]$	Martin and Hill (1987b)
	$k_6 = 1000\ M^{-1}\ s^{-1}$ (for low S(IV))	
NO_2	$k_7[NO_2(aq)][S(IV)]$	Lee and Schwartz (1983)
	$k_7 = 2 \times 10^6\ M^{-1}\ s^{-1}$	

[a]This is an alternative reaction rate expression for the low-pH region. Compare with (7.92) and (7.95).

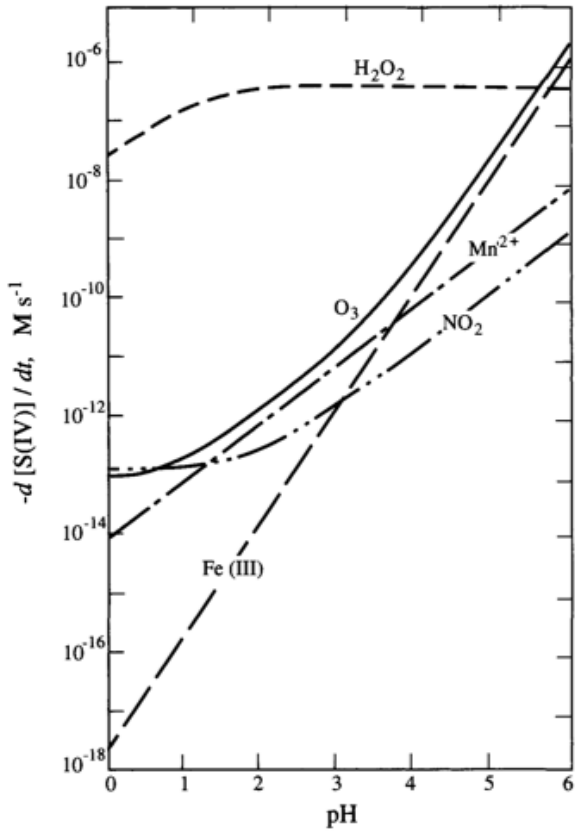

FIGURE 7.19 Comparison of aqueous-phase oxidation paths. The rate of conversion of S(IV) to S(VI) as a function of pH. Conditions assumed are $[SO_2(g)] = 5$ ppb; $[NO_2(g)] = 1$ ppb; $[H_2O_2(g)] = 1$ ppb; $[O_3(g)] = 50$ ppb; $[Fe(III)] = 0.3\ \mu M$; $[Mn(II)] = 0.03\ \mu M$.

Seinfeld and Pandis, 2006

Note that $\frac{dS(VI)}{dt} = -\frac{dS(IV)}{dt}$